

1  
2  
3  
4  
5  
6  
7  
8  
9  
10  
11  
12  
13  
14  
15  
16  
17  
18  
19  
20  
21  
22  
23  
24  
25  
26

# A universal DNA signature for the Tree of Life

Bruno A. S. de Medeiros<sup>1,2,3</sup>, Liming Cai<sup>4,5</sup>, Peter J. Flynn<sup>4</sup>, Yujing Yan<sup>4</sup>, Xiaoshan Duan<sup>4,6</sup>,  
Lucas C. Marinho<sup>4,7</sup>, Christiane Anderson<sup>8</sup>, and Charles C. Davis<sup>4</sup>

<sup>1</sup>Field Museum of Natural History, Chicago, Illinois, 60605, USA

<sup>2</sup>Department of Organismic and Evolutionary Biology, Museum of Comparative Zoology,  
Harvard University, Cambridge, Massachusetts, 02138 USA

<sup>3</sup>Smithsonian Tropical Research Institute, Panama City, Panama

<sup>4</sup>Department of Organismic and Evolutionary Biology, Harvard University Herbaria,  
Harvard University, Cambridge, Massachusetts, 02138 USA

<sup>5</sup>Department of Integrative Biology, The University of Texas at Austin, Austin, Texas, 78712  
USA

<sup>6</sup>College of Forestry, Northwest Agriculture & Forestry University, Yangling 712100,  
Shaanxi, China

<sup>7</sup>Departamento de Biologia, Universidade Federal do Maranhão, Av. dos Portugueses 1966,  
Bacanga 65080-805, São Luís, Maranhão, Brazil

<sup>8</sup>University of Michigan Herbarium, 3600 Varsity Drive, Ann Arbor, Michigan 48108, USA

**Corresponding authors:**

Bruno A. S. de Medeiros, Field Museum of Natural History, Chicago, IL, 60605; E-mail:  
[bdemedeiros@fieldmuseum.org](mailto:bdemedeiros@fieldmuseum.org)

27 Charles C. Davis, Department of Organismic and Evolutionary Biology, Harvard University  
28 Herbaria, Cambridge, MA 02138, USA; E-mail: [cdavis@oeb.harvard.edu](mailto:cdavis@oeb.harvard.edu)

29

30

# 31 Abstract

32 Species identification using DNA barcodes has revolutionized biodiversity sciences and  
33 society at large. However, conventional barcoding methods may lack power and universal  
34 applicability across the Tree of Life. Alternative methods based on whole genome  
35 sequencing are hard to scale due to large data requirements. Here, we develop a novel  
36 DNA-based identification method, varKoding, using exceptionally low-coverage genome  
37 skim data to create two-dimensional images representing the genomic signature of a  
38 species. Using these representations, we train neural networks for taxonomic  
39 identification. Applying a taxonomically verified novel genomic dataset of Malpighiales  
40 plant accessions, we optimize training hyperparameters and find the highest performance  
41 by combining a transformer architecture with a new modified chaos game representation.  
42 Remarkably, >91% precision is achieved despite minimal input data, exceeding alternative  
43 methods tested. We illustrate the broad utility of varKoding across several focal clades of  
44 eukaryotes and prokaryotes. We also train a model capable of identifying all species in  
45 NCBI SRA using less than 10 Mbp sequencing data with 96% precision and 95% recall and  
46 robust to sequencing platforms. Enhanced computational efficiency and scalability,  
47 minimal data inputs robust to sequencing details, and modularity for further development  
48 make varKoding an ideal approach for biodiversity science.

49  
50 **Keywords:** biodiversity science, computer vision, DNA barcoding, genomic signature,  
51 Malpighiaceae, natural history collections, neural networks, species identification,  
52 taxonomy

## 53 Introduction

54 For two decades, conventional DNA barcoding, which relies on standardized short  
55 sequences (400–800 bp) for species identification<sup>1–5</sup>, has enabled novel and massively  
56 scalable science spanning evolution<sup>4,6–9</sup>; ecology<sup>10–14</sup> and paleontology<sup>15–19</sup>. Practical  
57 applications of barcoding have also made major contributions to environmental health,  
58 including the ability to authenticate medicinal plants<sup>20</sup>, detect agricultural pests<sup>21</sup>, and  
59 monitor poaching and the trade of endangered species<sup>22–27</sup>. Despite these remarkable  
60 achievements, conventional DNA barcoding suffers from at least four limitations. First,  
61 barcodes are customized specifically for a taxon (e.g., plants, animals, and fungi), and  
62 therefore are not universal. For example, commonly used plant barcodes from chloroplast  
63 genes such as *matK* and *rbcL* cannot be applied as barcodes for all plants<sup>28,29</sup>, or for animals  
64 and fungi. Second, conventional barcode loci may fail to distinguish closely related taxa, a  
65 pervasive shortcoming in plants<sup>2,30</sup>. Third, reliance on a single locus may lead to spurious  
66 results in the case of complex evolutionary scenarios such as hybridization in deep or  
67 shallow time<sup>31–34</sup>. And fourth, the necessary comparison of homologous genes may fail  
68 when PCR primers are not universal<sup>35</sup>, the source DNA is fragmented<sup>27</sup>, or paralogy and the  
69 presence of pseudogenes confounds accurate orthology assessments<sup>36,37</sup>.

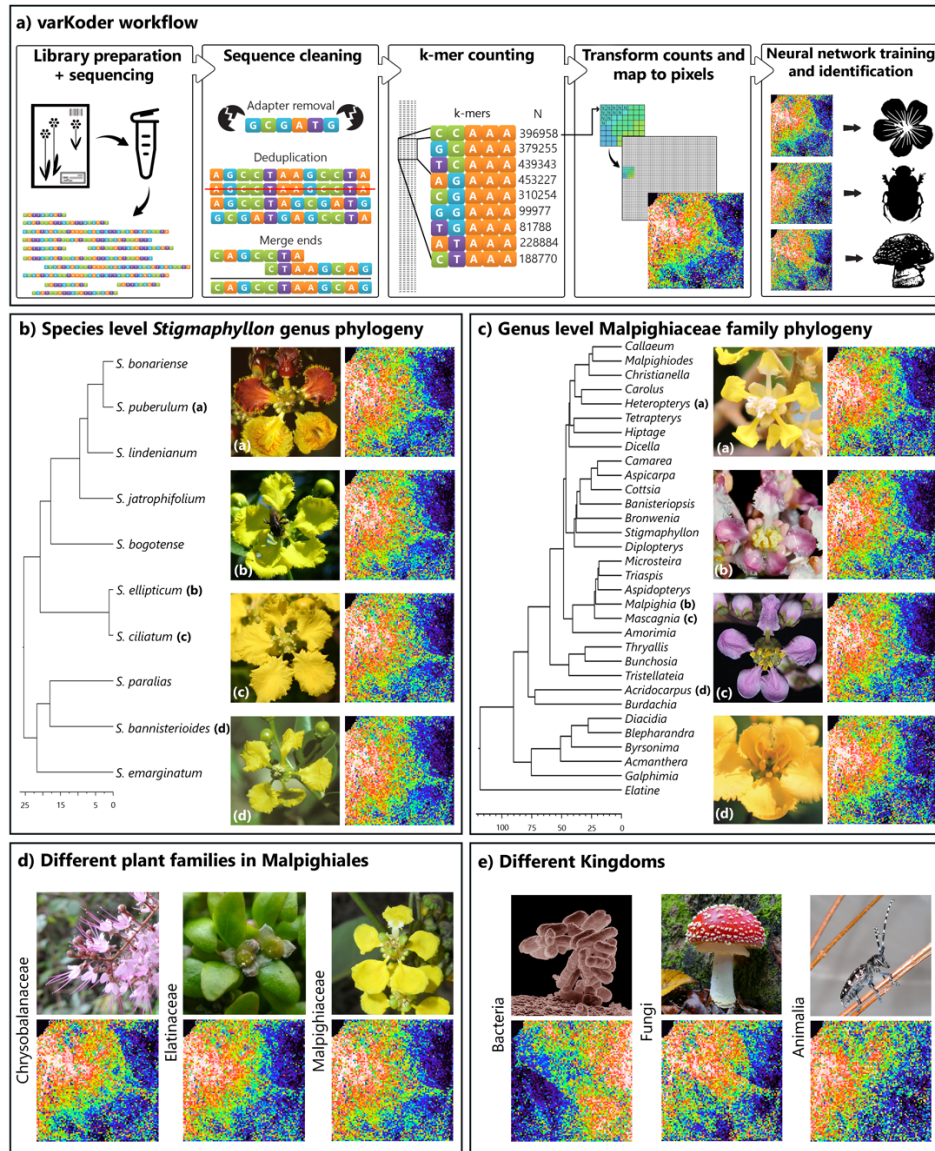
70  
71 Newer alternatives to conventional barcoding have begun to address these challenges by  
72 leveraging high-throughput sequencing and machine-learning powered by deep neural  
73 networks. High-throughput sequencing facilitates more comprehensive assessments of  
74 total genomic space<sup>38,39</sup>. For example, presence and absence patterns among short DNA  
75 sequences (k-mers) from low-coverage reads (i.e., genome skims) can estimate overall  
76 sequence distances, bypassing genome alignments entirely as implemented in *Skmer*<sup>40</sup>.  
77 Machine learning enables more complex sequence comparisons than conventional methods  
78 that rely on homology and simple metrics<sup>41</sup>. Machine-learning models can cluster DNA  
79 sequences without supervision<sup>42,43</sup> or classify sequences based on reference datasets<sup>44–49</sup>.  
80 In particular, neural networks are exceptionally powerful for sophisticated computer-  
81 vision tasks, such as image classification<sup>50</sup>. Thus, the combination of low-coverage genome

82 skimming data and neural networks holds enormous promise for accurate and scalable  
83 DNA barcoding, but its potential has yet to be fully realized<sup>39</sup>.

84

85 Genomes differ substantially in many features beyond the simple nucleotide divergence  
86 commonly used in conventional barcoding, but these genomic features have been  
87 overlooked in species identification<sup>31,51-55</sup>. We propose that (1) relevant genomic features  
88 can be captured by nucleotide composition with short k-mer counts and very small  
89 sequence coverage; and (2) these counts can be used to distinguish species and higher taxa  
90 efficiently and accurately using machine learning. Prior work on k-mer-based  
91 representations of genome composition (i.e., genomic signatures) has shown high accuracy  
92 can be achieved with high-coverage data or a large number of replicates per taxon,  
93 particularly for identification at higher taxonomic ranks<sup>42-47,56-63</sup>. However, given the  
94 millions of existing species and the sparse genetic data available, a practical scalable  
95 method would require: (1) consistently high accuracy despite limited evolutionary  
96 divergence; (2) fast computations; and (3) high accuracy with small training datasets (both  
97 in number of samples and DNA data per sample). Here we developed a novel genomic  
98 signature method, which we call **varKoding**, that integrates very low-coverage genome  
99 skim data with optimized training of machine-learning models using two-dimensional  
100 images representing genome composition (**Figure 1A**). We focus on images as forms of  
101 genomic representation since they can be easily stored and accessed across computing  
102 platforms, annotated with metadata and readily employed as input data in popular  
103 machine learning frameworks such as pytorch<sup>64</sup>. Specifically, our method relies on raw  
104 unassembled genomic reads sampling a very small fraction of a genome, since sequence  
105 assembly is costly both in terms of DNA sequencing and computation<sup>40,58</sup> and sparse  
106 sampling of genomic regions may be sufficient to summarize its features<sup>39</sup>. To develop and  
107 optimize varKoding for accurate species identification, we generated a *de novo* genome  
108 skim dataset including hundreds of samples derived primarily from historical herbarium  
109 specimens for the diverse plant genus *Stigmaphyllon* (Malpighiaceae), which has received  
110 extensive phylogenetic and taxonomic treatment<sup>65-69</sup>. Next, we explored the utility of  
111 varKoding and compared it to alternatives at different phylogenetic depths from families to

112 species within the flowering plant order Malpighiales (Malpighiaceae, Chrysobalanaceae,  
 113 and Elatinaceae). Finally, we demonstrate the scalability of varKoding and its potential  
 114 application in forensics and related fields by testing it on (1) species-level datasets from  
 115 fungi, plants, animals, and bacteria; (2) massive datasets retrieved from the NCBI sequence  
 116 read archive (SRA); and (3) a previously published environmental DNA (eDNA) dataset.  
 117



118

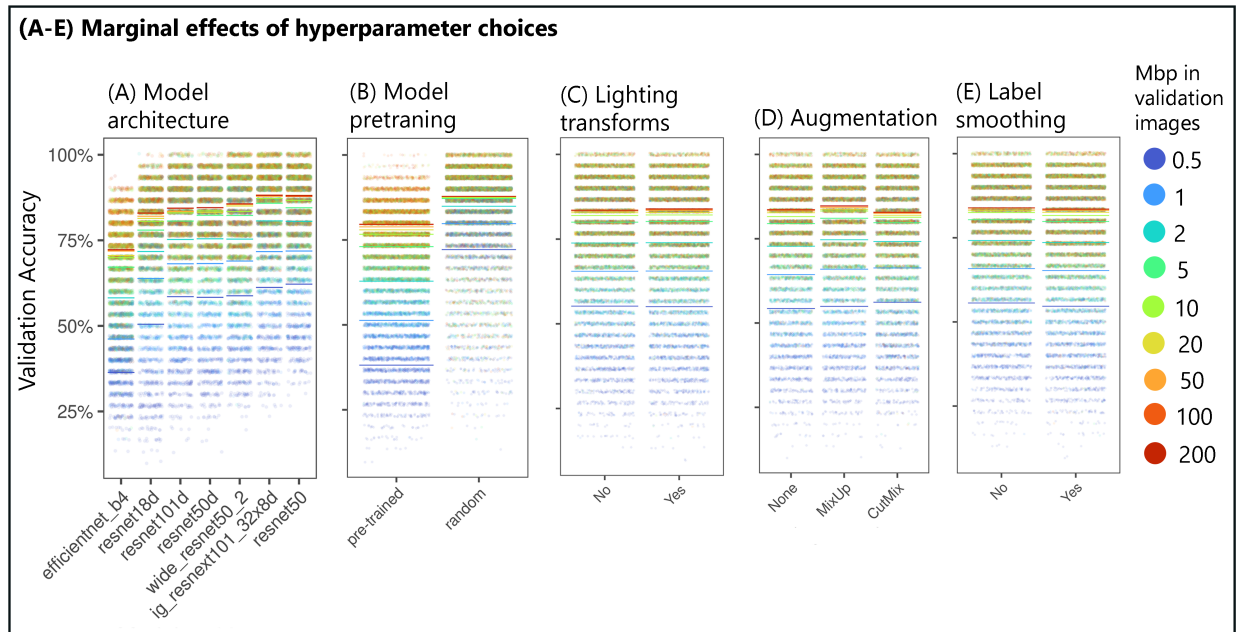
119 **Figure 1.** Overview of varKoding. (A) Image generation workflow, depicting varKodes.  
 120 Images are natively grayscale, but here they are mapped to a rainbow color scale for  
 121 increased contrast. (B) Phylogeny and example varKodes of *Stigmaphyllon* species. (C)

122 Phylogeny and example varKodes of Malpighiaceae genera including their closest outgroup  
123 (*Elatine*, Elatinaceae). Time trees in 1B and 1C were derived from an ongoing family-wide  
124 phylogenomic investigation of the family Malpighiaceae (C. C. Davis personal  
125 communication) using methods and fossil constraints described in Cai et al.<sup>66</sup>. **(D)**  
126 Examples of varKodes from across plant families of Malpighiales, and **(E)** across kingdoms.  
127 Chronograms depicted for each representative set with timelines in millions of years (Myr)  
128 at the bottom of **B** and **C**.

## 129 **Results and Discussion**

### 130 **Genomic signature images can be classified with generalized neural networks**

131 We first generated a novel kind of image representation of a genomic signature based on  
132 raw reads, which we termed a **varKode**. varKodes map k-mers onto pixels of a 2-D image  
133 based on their similarity and represent ranked k-mer frequencies as pixel brightness.  
134 Variation in varKodes can be small but remain visually perceptible among species **(Figure**  
135 **1B)** and genera **(Figure 1C)**. Variation is more striking among higher levels of phylogenetic  
136 divergence, such as between families in the order Malpighiales **(Figure 1D)** or different  
137 kingdoms of eukaryotes and prokaryotes **(Figure 1E)**. We expected, therefore, that neural  
138 network architectures developed for image classification, (e.g., deep residual networks,  
139 resnets<sup>70</sup> or vision transformers, ViT<sup>71,72</sup>) would be able to differentiate varKodes.  
140

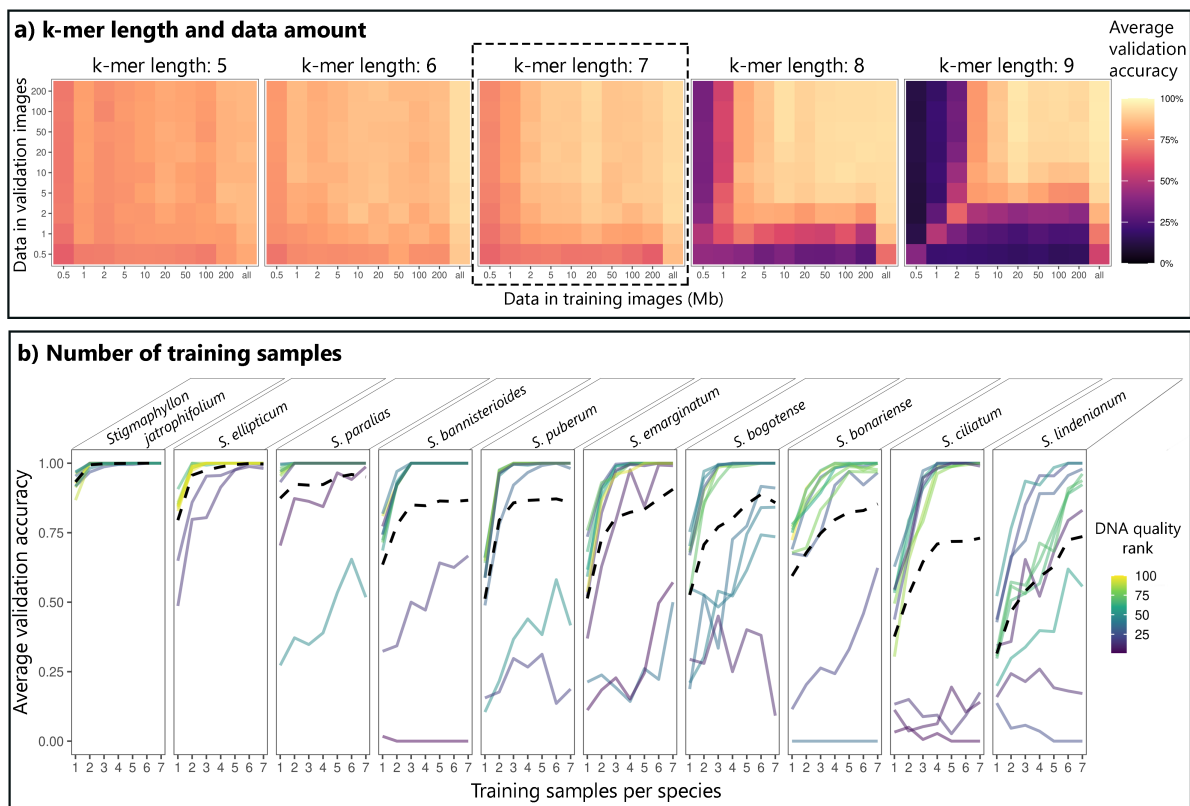


141  
 142 **Figure 2.** Marginal effects of neural network model and training options. Dots represent  
 143 individual replicates, and bars depict averages. All parameters were identified to be  
 144 significant in a linear model: more complex model architectures, lighting transformations,  
 145 and augmentation methods *MixUp* and *CutMix* improved accuracy. However, pretraining  
 146 with large image datasets and label smoothing decreased accuracy.

147  
 148 We first optimized hyperparameters and training conditions to maximize accuracy for  
 149 species-level identification of *Stigmaphyllon*. We identified that varKodes depicting k-mer  
 150 length = 7 struck a good balance between accuracy and the amount of input sequence data  
 151 (**Figure 3A**). Furthermore, models trained with augmented data from several subsampled  
 152 sequences drawn from each individual exhibited substantially better performance (**Figure**  
 153 **3A**). A linear model demonstrated that neural network architectures and training methods  
 154 designed for image classification of photographs<sup>70,73–76</sup> are extremely useful for varKode-  
 155 based identification. Specifically, we observed increased accuracy with more parameter-  
 156 rich neural network architectures (*ResNeXt101*<sup>77</sup>, among those tested), augmentation with  
 157 lighting transformations, *CutMix*<sup>76</sup> and *MixUp*<sup>75</sup>. Label smoothing<sup>78</sup> and pretraining models  
 158 on generalized photographs decreased accuracy (**Figure 2**). Contrary to the widely held  
 159 idea that deep neural networks require very large training datasets<sup>60,79</sup>, the  
 160 aforementioned approaches enabled training with very modest data amounts: four



161 biological replicates per taxon was sufficient for 100% median accuracy (**Figure 3B**).  
 162 Errors in species-level identification were concentrated among sequences derived from  
 163 herbarium samples that demonstrated evidence of DNA damage, as is sometimes reported  
 164 for ancient DNA<sup>80</sup> (**Figure 3B**). However, including low-quality training samples slightly  
 165 decreased mean validation accuracy—from 73% to 71%—for low-quality validation  
 166 samples, but had no effect on high-quality validation samples (89–90% mean accuracy,  
 167 **Figure 4**).  
 168

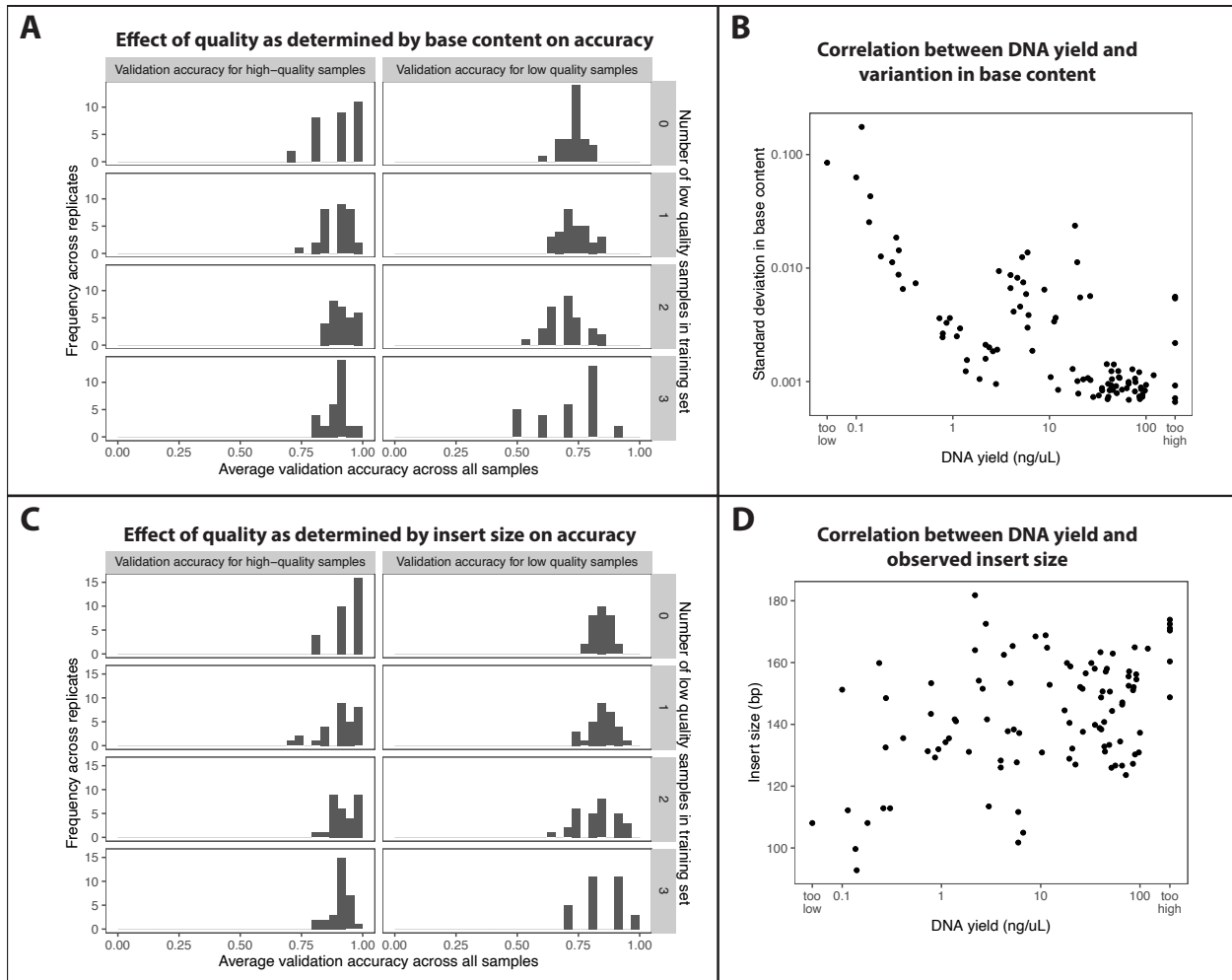


169

170 **Figure 3. Neural network training of varKodes for species identification. (A)** Effect of  
 171 k-mer length and input data amount used to produce varKodes on validation accuracy.  
 172 Longer k-mers increase accuracy when more data are used. Mixing varKodes subsampled  
 173 from different amounts of data improves accuracy. Box with dashed line (k-mer length = 7)  
 174 strikes a good balance between model accuracy and amount of required data. **(B)**  
 175 Validation accuracy improves with increased number of training samples per species, but  
 176 even 3–4 samples are sufficient in most cases for achieving high accuracy. Each solid line

177 represents one sample, colored by DNA quality (i.e., variation in base pair frequencies).  
 178 Higher rank indicates better quality. Dashed lines represent averages across all samples.

179



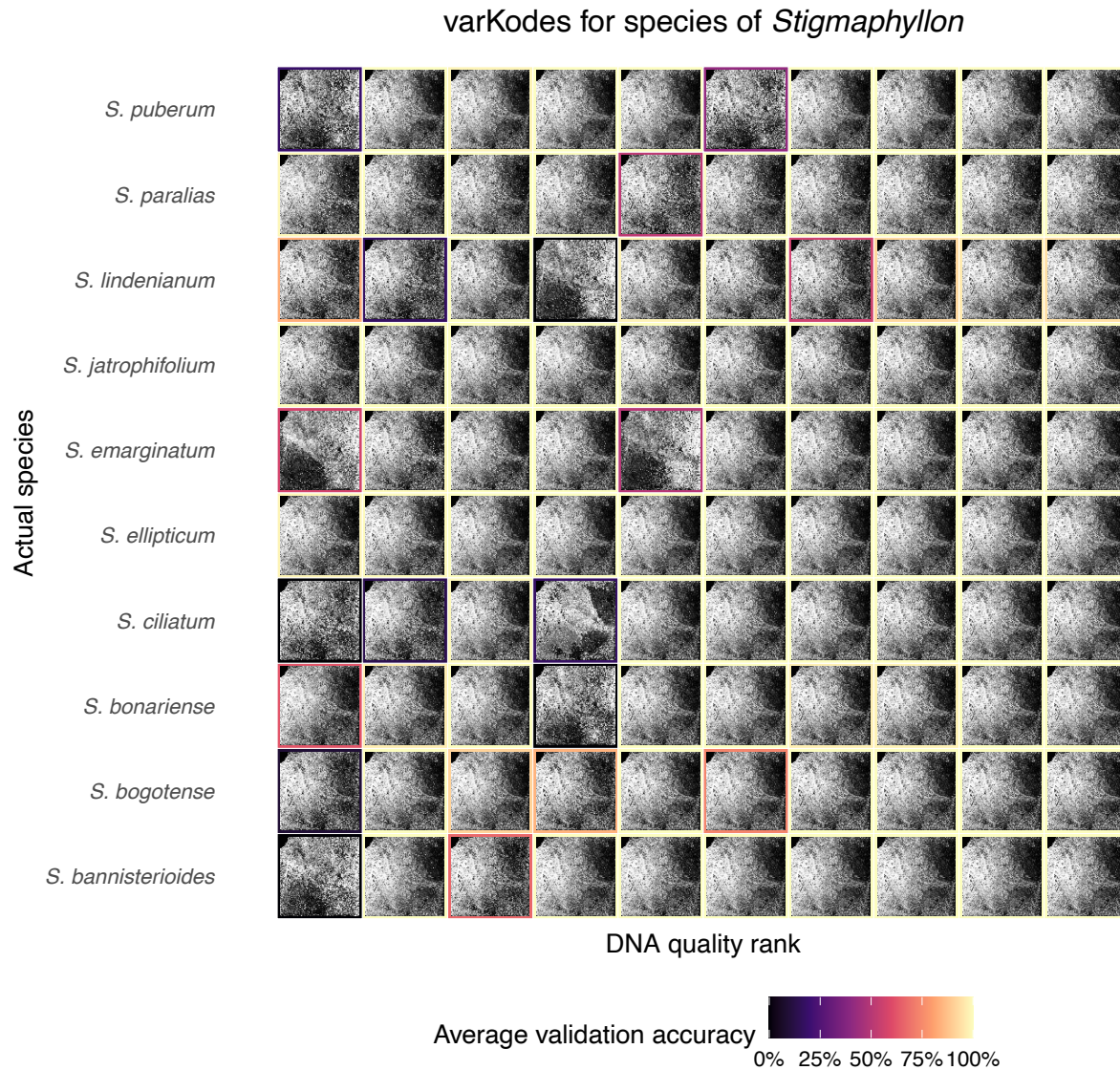
180

181 **Figure 4.** Effect of the inclusion of low-quality training samples, inferred from variation in  
 182 base pair content (A, B) or insert size (C, D). Increasing the fraction of samples in the  
 183 training set that were low-quality did not strongly affect the average validation accuracy,  
 184 but it increased dispersion. Low-quality samples are the four samples with highest  
 185 variation in base-pair content or shortest insert size in raw reads for each species. Panels **B**  
 186 and **D** show the correlation of each quality metric with DNA extraction yield.

187

188

189 We hypothesized that lower-quality samples shared similar sequences resulting from  
190 common patterns of DNA damage and greater levels of microbial or human contaminants,  
191 resulting in spurious similarities in varKodes (**Figure 5**). Contaminants also are thought to  
192 increase errors in other genome skim methods<sup>81</sup>. To mitigate this problem, we applied  
193 multi-label classification<sup>82</sup> to our neural network models. Although single-label  
194 classification models always return a single prediction (that is, an inferred label), multi-  
195 label models can return zero or more predictions, avoiding spurious results when there is  
196 uncertainty. For a set of samples with known labels used for validation, a prediction is a  
197 true positive if the predicted label matches the actual label, and a false positive if not.  
198 Failure to predict an actual label is deemed a false negative. For each validation sample, we  
199 summarized predictions as (1) correct (true positives only); (2) incorrect (false positives  
200 only); (3) ambiguous (multiple predictions, including true and false positives); or (4)  
201 inconclusive (i. e. no prediction above the confidence threshold). For each test, we  
202 summarized results across all validation samples using two metrics: precision (the sum of  
203 all true positives divided by the sum of all true and false positives) and recall (the sum of all  
204 true positives divided by the sum of all true positives and negatives).  
205



206

207 **Figure 5.** Low-quality DNA may lead to spurious patterns of similarity in varKodes.

208 Samples with lower quality show varKode patterns divergent from their species more often

209 than high-quality ones. These divergent patterns may be similar between low-quality

210 samples across species. These samples also show reduced validation accuracy in a single-

211 label model. For each sample, we show the varKodes produced from all DNA data available.

212 Within each species, samples are organized from lowest (left) to highest (right) DNA

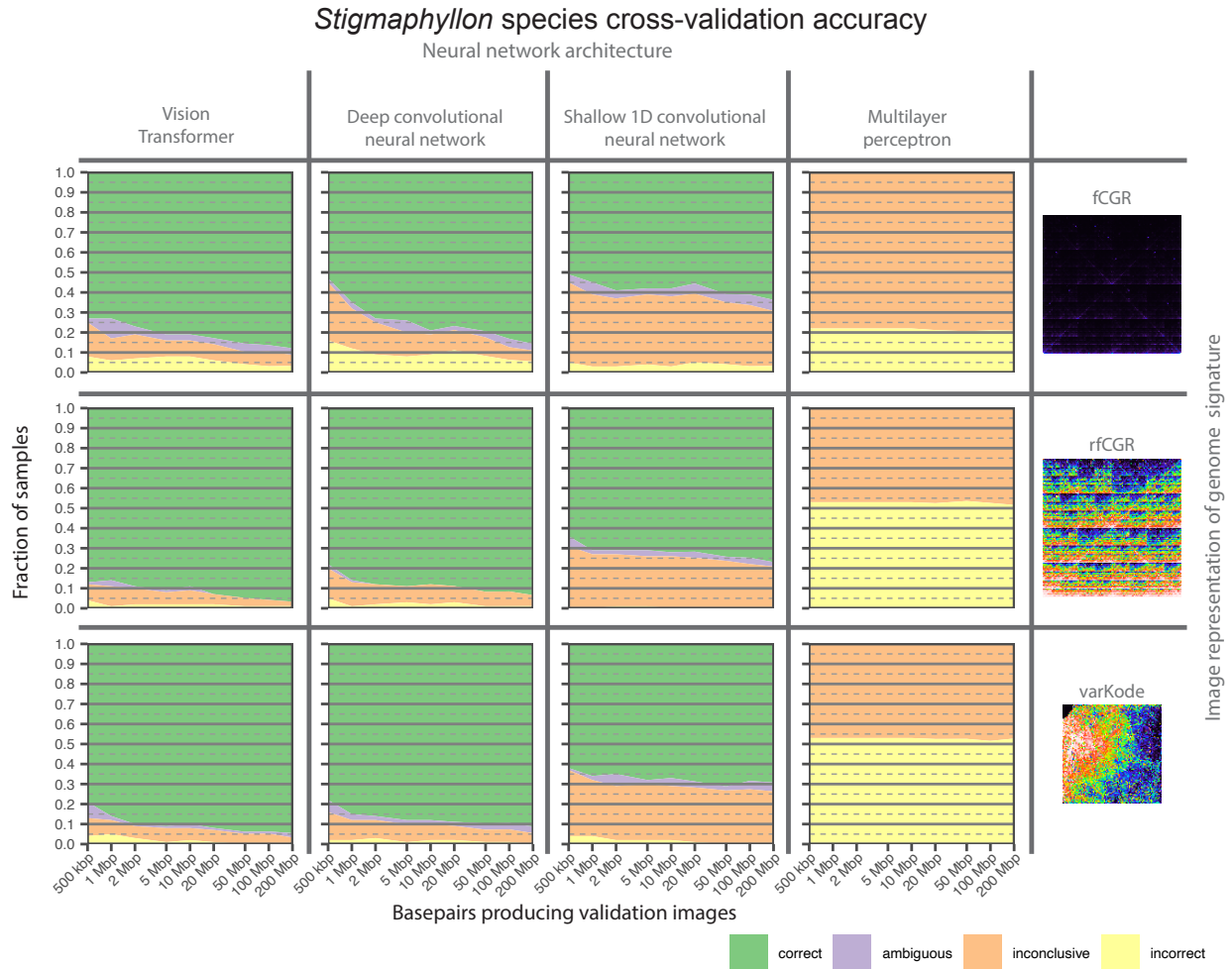
213 quality. Bounding boxes around each sample indicate the average validation accuracy

214 across 30 random replicates with 7 training samples per species.

215

216 After optimizing these training conditions, we directly compared varKodes to an existing  
217 method of genomic signature representation: the frequency chaos game representation  
218 (*fCGR*)<sup>56,59</sup>. In *fCGRs*, k-mers are mapped to pixels based on their oriented sequence and  
219 pixel brightness represents the rescaled k-mer frequency. To isolate the effects of pixel  
220 mapping and brightness, we created a new representation combining *fCGR* mapping with  
221 *varKode* ranked frequency transformation (*rfCGR*). Because raw sequence reads often  
222 contain artifactual k-mers at very high frequencies, especially when low-quality DNA is  
223 used to construct libraries, we hypothesized that *rfCGRs* would perform better than *fCGRs*,  
224 where pixel brightness is linearly scaled to k-mer counts. By directly comparing these 3  
225 kinds of representation combined with four neural network architectures, including (1)  
226 two previously employed with *fCGRs*<sup>42,44,60</sup>, (2) the optimal architecture in our initial tests  
227 (ResNeXt101<sup>77</sup>), and (3) a Vision Transformer (ViT<sup>71,72</sup>), we found that ViT combined with  
228 *rfCGR* representation maximizes performance (**Figure 6**). While *fCGRs* have been initially  
229 proposed as tools to study single sequences<sup>56</sup>, here we focus all of our comparisons on the  
230 task of supervised classification-based genomic composition from very low coverage  
231 sequencing. A multilayer perceptron, as employed in previous work<sup>42,60</sup>, could not identify  
232 any species correctly here (**Figure 6**). Similarly, a previously employed shallow 1D  
233 convolutional neural network<sup>44</sup> underperformed more complex architectures (**Figure 6**).  
234 *fCGR* showed much higher error rates than either *rfCGR* or *varKodes*, which yielded similar  
235 results but with slightly higher accuracy for *rfCGR* (**Figure 6**). These results indicate that  
236 deep complex neural networks, while not explicitly developed for genomic signature, are  
237 necessary to extract features from very low-coverage data and distinguish closely related  
238 species. Moreover, the method of k-mer frequency data transformation seems more  
239 consequential than the mapping of k-mers to pixels for the performance of different image  
240 representations. Due to its higher performance, we adopt the combination of *ViT* and  
241 *rfCGRs* for subsequent tests.

242



243

244 **Figure 6.** Effect of image representation and neural network architecture on cross-  
 245 validation accuracy of species identification in *Stigmaphyllon*. One example for each image  
 246 representation is shown, drawn from the same DNA data (SRA accession XXXX) and  
 247 mapped to a rainbow color scale for increased contrast. See text for details on  
 248 architectures.

249

250 In summary, we developed and tested a robust and scalable method of DNA barcoding  
 251 capable of training with small amounts of data, and implemented it in the ***varKoder***  
 252 software, which can process sequence data, train an image-classification neural network  
 253 using varKodes or rfCGRs, query new data with a trained neural network, and convert  
 254 between the alternative k-mer mappings. These tasks are accomplished with widely used  
 255 tools for sequence processing<sup>83–87</sup> and for neural network training<sup>64,88–90</sup>.



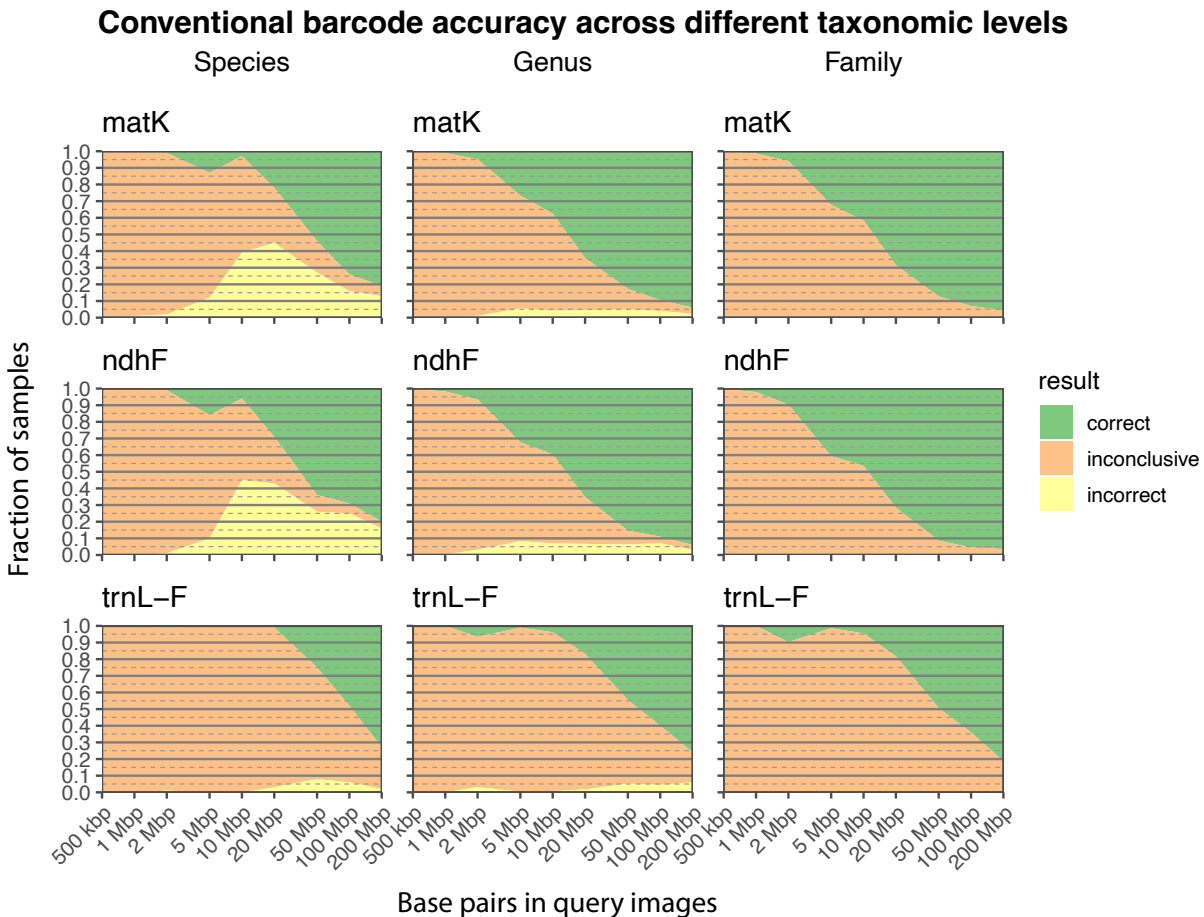
**268 varKodes are highly accurate for identification of species, genera, and families**

269 To test *varKoder* under a real-world scenario with heterogeneous data (e.g., large numbers  
270 of taxa, multiple replicates per taxon, varying sequence depth and sample quality), our *de*  
271 *novo* genomic data set included 287 accessions: 100 samples of *Stigmaphyllon* from our  
272 initial development outlined above, plus additional genera in the families Malpighiaceae  
273 (31 genera; 151 samples), Chrysobalanaceae (8 genera; 30 samples), and Elatinaceae (1  
274 genus; 6 samples) in the order Malpighiales. We found high cross-validation accuracies for  
275 species identity of *Stigmaphyllon* (87.0–96.7% correct, 94.6%–98.9% precision, 88.0%–  
276 96.7% recall depending on data input amount; **Figure 7A**). Most errors were inconclusive  
277 predictions (2.2–10%), instead of ambiguous (0–3%) or incorrect (1–4%) predictions.  
278 *varKoder* is robust to the amount of input sequence data necessary for model training,  
279 performing well even at the lower range of input data (**Figure 7A**). Assuming an average  
280 genome size of about 2 Gbp for the average species of Malpighiaceae<sup>91</sup>, the 500Kbp–  
281 200Mbp of data used here represented exceptionally low coverages of about  $\sim 0.0002\times$  –  
282  $0.107\times$ . Such low coverages imply that we are likely not comparing homologous regions  
283 across taxa, but rather more general genomic properties that can be inferred from  
284 extremely sparse sampling. Moreover, when compared to cross-validation accuracies of  
285 alternative barcoding methods, *varKoder* accuracy is higher than *Skmer*, which showed  
286 46% correct predictions (57.5% precision, 46% recall) with minimal data amounts and  
287 peaked at 79.1% for the larger data amounts (80% precision, 79.1% recall, **Figure 7A**). On  
288 the other hand, conventional barcodes including individual plastid genes and nuclear  
289 ribosomal ITS regions performed well for both BLAST-based (25–97% correct, 66.6–97.3%  
290 precision, 25–97% recall depending on the gene) and phylogenetic-based (94–95% correct,  
291 >99% precision, 97.2–98.4% recall for concatenated matrices) approaches when at least 50  
292 Mbp of data was provided (**Figure 7A, Figure 8**). However, these results were much worse  
293 when <50 Mbp of data were available (down to zero correct for BLAST). In this case,  
294 unsuccessful locus assembly leading to inconclusive predictions as the primary reason for  
295 the failure (**Figure 7A, Figure 8**), so we expect that alternative methods to BLAST (e.g. <sup>48,92</sup>)  
296 would not perform substantially better. Finally, an unsupervised clustering method based  
297 on neural networks applied to *fCGRs* (*iDeLUCS*<sup>93</sup>) reached 24–60% clustering accuracy



298 depending on input data amount when prompted to cluster *Stigmaphyllon* sequences into  
 299 10 groups. In summary, *varKoder* reaches much higher accuracy for species determination  
 300 than existing methods for unprecedentedly small amounts of data and demonstrates  
 301 similar accuracies when greater amounts of sequence data are available.

302  
 303

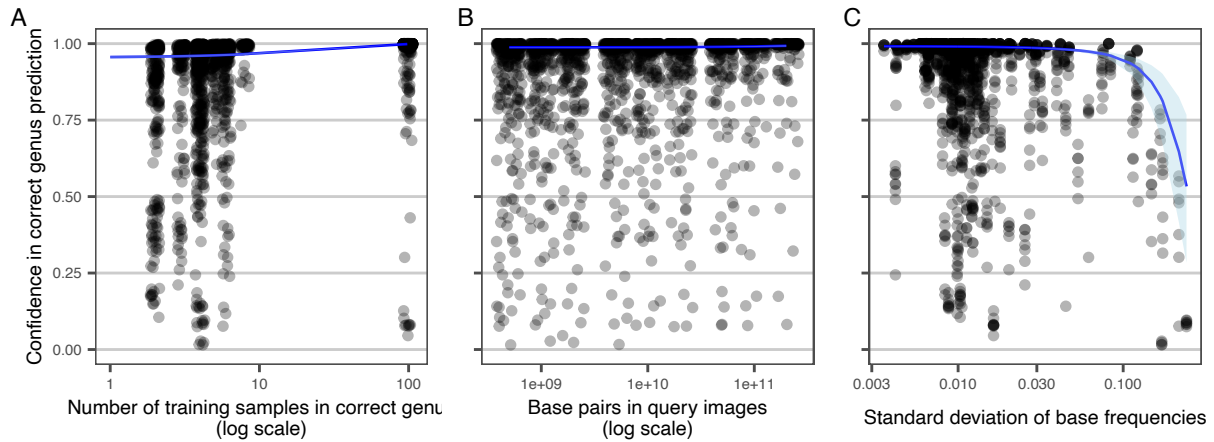


304  
 305 **Figure 8.** Accuracy of conventional barcode loci for species, genera and families within the  
 306 Malpighiales.

307  
 308 Genus-level identification yielded similar high accuracies with *varKoder* (86.1–93.3%  
 309 correct, 97.2%–97.7% precision, 86.4%–94.7% recall depending on input amount, **Figure**  
 310 **7B**), but with a higher rate of inconclusive predictions (4.5–11.5%). A linear model  
 311 demonstrated that this higher uncertainty can be attributed to two factors: (1) samples

312 exhibiting higher levels of DNA damage in genera other than *Stigmaphyllon*; and (2) genera  
313 trained with fewer replicates (e.g., down to 3 samples for some genera; **Figures 9-10**).  
314 Despite this trend, the vast majority of genera with fewer replicates and lower DNA quality  
315 can still be correctly predicted, resulting in the >97% prediction and >86% recall across  
316 the whole dataset. Additionally, samples within genera share fewer genetic similarities  
317 than samples within species, which likely poses a more challenging classification problem.  
318 However, the incorrect rate was very small in all cases (0.7–2.1%), with most errors being  
319 inconclusive or ambiguous predictions. In contrast, *Skmer* exhibited better performance  
320 when larger amounts of data were used (99.2% correct, 99.2% precision, 99.2% recall for  
321 200 Mbp), but performed poorly for lower amounts of data like those commonly generated  
322 from genome skim experiments (58.2% correct, 58.2% precision, 58.2% recall for 500  
323 Kbp) (**Figure 7B**). Genus-level identifications using conventional barcodes in a  
324 concatenated phylogeny were up to 98.1% correct (99.2% precision, 97.2% recall) when  
325 a large amount of data (200 Mbp) was available (**Figure 7B**). But like its application at  
326 species-level identification, most predictions were inconclusive when less than 20 Mbp  
327 reads were used (**Figure 7B**). Although genome skimming can be used to sequence  
328 conventional barcodes, they are more often obtained with amplicon sequencing, which has  
329 failure rates ranging from 15–75% even with highly optimized protocols<sup>94</sup>, leading to an  
330 even higher number of inconclusive predictions. At the family level, *Skmer* and *varKoder*  
331 had near-perfect accuracy across all data amounts (>97% correct), while conventional  
332 barcodes performed well when there were sufficiently large amounts of data (**Figures 8,**  
333 **11**).  
334

## Factors affecting varKode prediction accuracy



335

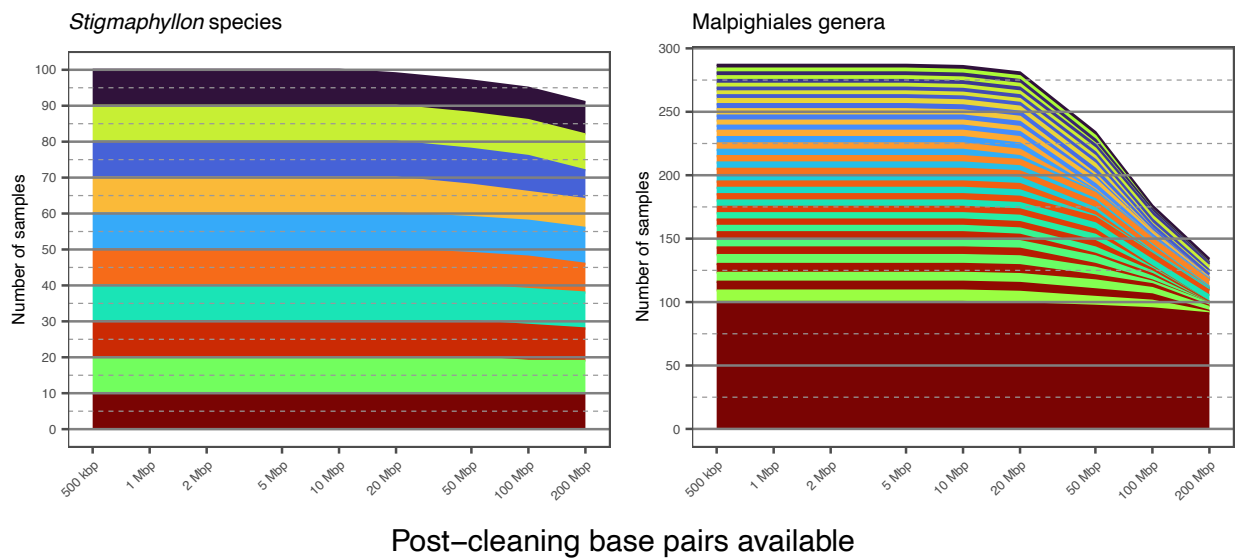
336 **Figure 9.** Predictors of confidence in correct genus. A) Confidence increases with more

337 training samples per genus. B) Amount of data per validation image has little effect. C)

338 Validation samples with low quality have lower confidence.

339

## Number of samples available for different data amounts



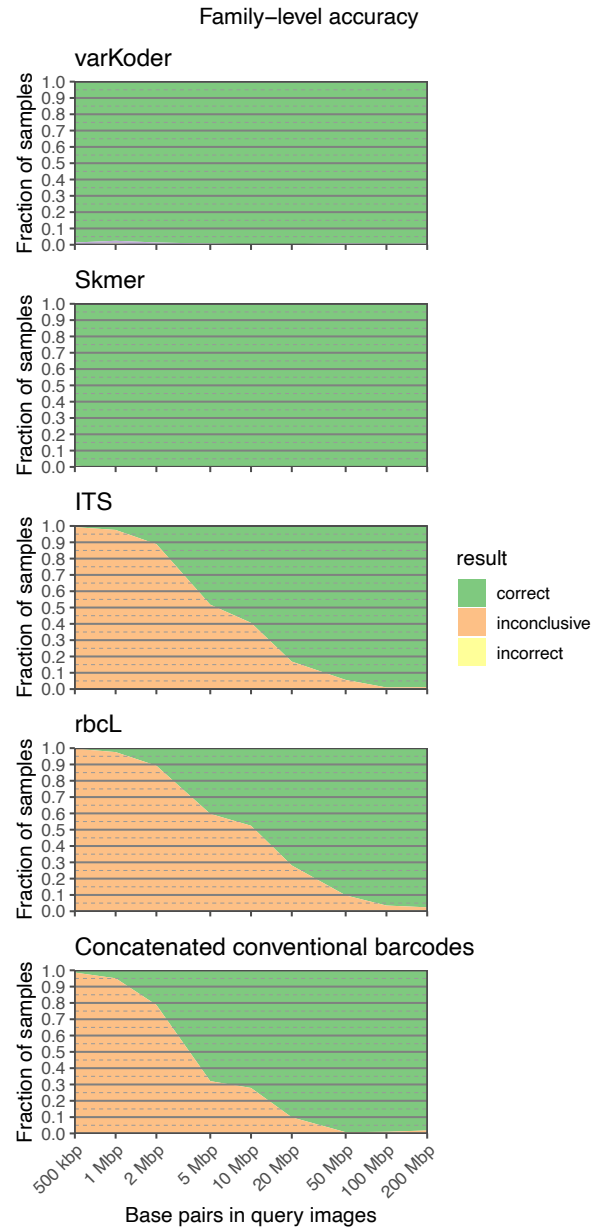
340

341 **Figure 10.** Number of samples available for different data amounts in the Malpighiales and

342 Eukaryote families datasets. Arbitrary colors are assigned to individual taxa.

343

344



345

346 **Figure 11.** Comparison of *varKoder*, *Skmer*, and conventional barcode accuracy for  
 347 identifying families of Malpighiales.

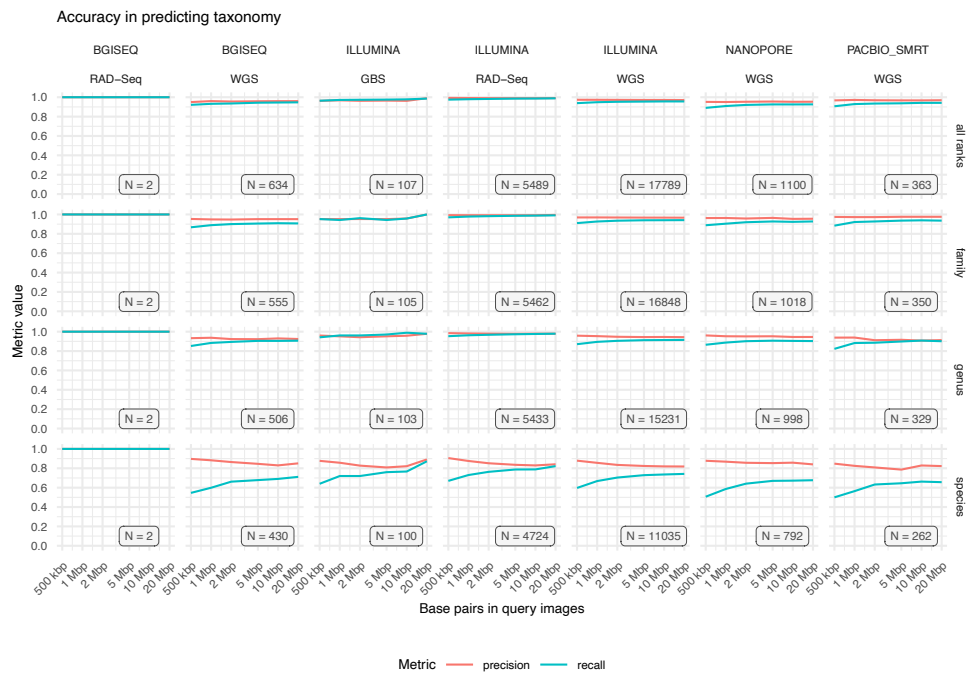
348

349 **varKodes are universal and scalable across the Tree of Life**

350 To further test the universality of varKodes, we expanded to sequencing data from diverse  
 351 clades of plants, fungi, animals, and bacteria (**Figure 7C**). These tests included species-level  
 352 identification in insects (*Bembidion* beetles<sup>54,95</sup>) and lichen-forming fungi

353 (*Xanthoparmelia*<sup>96</sup>), species and infra-specific taxon identification in coralroot orchids

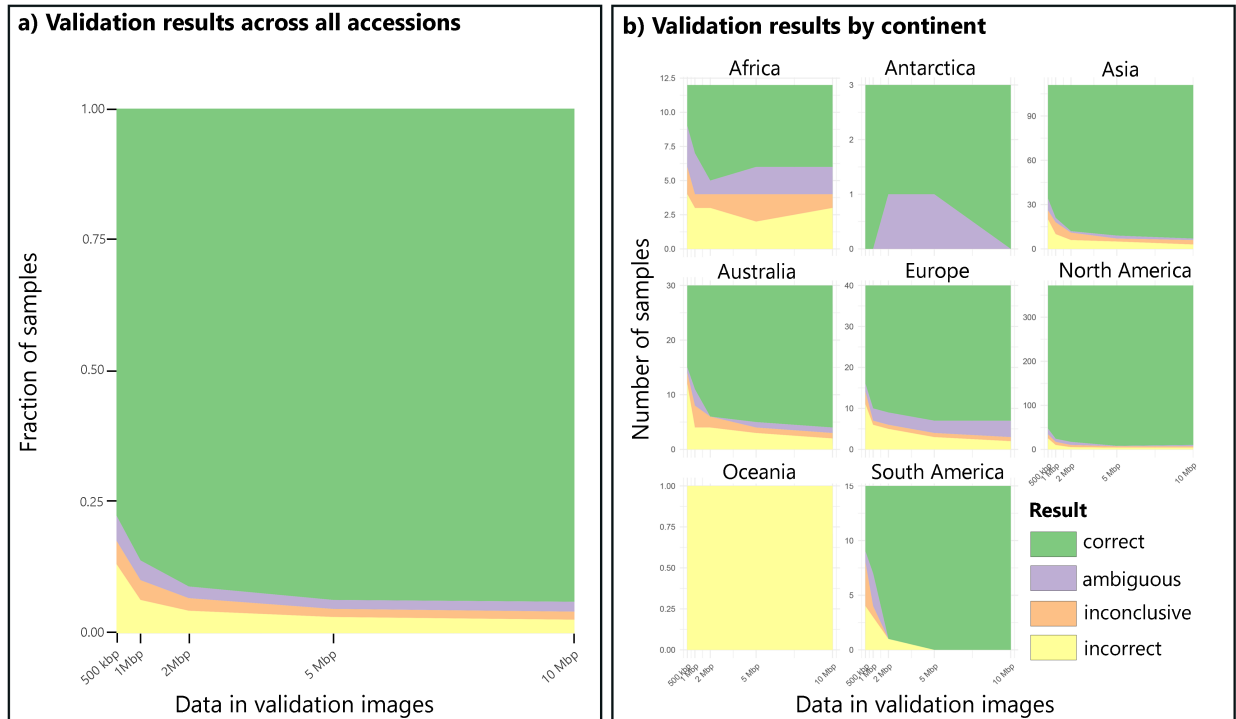
354 (*Corallorhiza*<sup>97</sup>), and clinical isolate identification of strains of human pathogenic bacteria  
 355 (*Mycobacterium tuberculosis*<sup>98</sup>). In all cases, we tested the performance of *varKoder* on taxa  
 356 included in the training set and on taxa not included in the training set. We identified  
 357 perfect species identification (100% correct, 100% precision, 100% recall) for beetles and  
 358 coralroot orchids included in the training set. For bacteria, 5.6% of the validation set  
 359 returned ambiguous predictions; the remaining samples were correctly identified (94.7%  
 360 precision, 100% recall). In lichen-forming fungi, which include DNA from both the fungal  
 361 and algal partners, and thus are more challenging, 10% of the test samples returned  
 362 incorrect predictions and another 10% were inclusive; the remainder were correct (89%  
 363 precision, 80% recall). For all cases, species or varieties not included in the training set  
 364 generally resulted in inconclusive results, with a minority yielding incorrect predictions  
 365 **(Figure 7C)**. Precision and recall using varKodes instead of *rfCGRs* were very similar for all  
 366 four datasets.  
 367



368  
 369 **Figure 12.** *varKoder* performance in predicting taxonomy for all data on SRA. Sample sizes  
 370 refer to the number of validation accessions available for each combination of platform,  
 371 sequencing strategy and taxonomic rank.  
 372

373  
374  
375  
376  
377  
378  
379  
380  
381  
382  
383  
384  
385  
386  
387  
388  
389  
390  
391  
392  
393  
394  
395  
396  
397  
398  
399  
400  
401  
402

Finally, we tested the scalability of varKodes in three large-scale datasets: (1) all 861 eukaryotic families with Illumina data on NCBI SRA, (2) all taxa with multiple accessions on NCBI SRA, including different sequencing platforms and library strategies (254,819 accessions and 14,151 taxa across all taxonomic ranks), and (3) a previously published dataset of 2916 soil eDNA samples from all seven continents<sup>99</sup>. Owing to NCBI download speed bottlenecks, we restricted varKode construction to a very limited maximum of 10 Mbp of DNA data in the former 2 cases. The family-level eukaryote data achieved a rate of correct predictions of 65.2–81.3% across all kingdoms when families were included in the training set (**Figure 7D**), with most errors being inconclusive predictions (17.5–33.1%). Precision varied from 95.3% to 97.3% and recall from 67.9% to 78.3%. Similarly to the species- and variety-level exercise, families not included in the training set often yielded inconclusive predictions (**Figure 7D**), suggesting a potential for varKoding to be used as a discovery tool when reasonably well-sampled training data sets are available. The expanded data with all taxa from NCBI SRA revealed that varKoding is robust to sequencing platform and library preparation method (**Figure 12**). Predictions at the family level or pooled for all the taxonomic hierarchy are accurate regardless of sequencing details (>94% precision, >86% recall). The much higher accuracy when compared to the dataset based on Eukaryotic families alone may be an effect of a completely random validation set instead of stratified by family, resulting in higher representation of commonly sampled families. At the genus and species level, results are more dependent on the sequencing method (**Figure 12**). For genera, precision/recall using 10Mbp of data varies from 90.8%/90.8% with whole genome shotgun libraries in PacBio to 97.9%/97.6% with genotype-by-sequencing in Illumina. Finally, the eDNA data shows promise in using varKoding to identify the geographical origin of an environmental sample (**Figure 13**): in the validation set, at 10Mbp of DNA data, 94.0% of the samples had continent correctly identified, with 2.6% being incorrect, 1.9% being ambiguous, and 1.5% being inconclusive (84.7% prediction, 84.5% recall). Precision and recall using varKodes instead of *rfCGRs* were very similar for both datasets.



403

404 **Figure 13.** Varkoder performance in identifying the geographical origin of a soil  
 405 metabarcoding sample. A) Performance across the whole dataset. B) Performance for each  
 406 continent.

407

408 A single model classifying all of life is not possible with conventional barcodes. *Skmer*, the  
 409 state-of-the-art genome skimming alternative, cannot be scaled to a dataset of this size: our  
 410 attempt to apply it to Eukaryote families could not be finished after more than 40 days  
 411 using 32 high-performance computing cores. In general, conventional barcodes, when  
 412 derived from genome skimming data, require memory- and processor-intensive sequence  
 413 assembly, and *Skmer* relies on pairwise all-by-all sample comparisons; its computing time  
 414 and required storage both increase quadratically with the number of samples. Neural  
 415 network models, on the other hand, have a fixed size, independent of the number of  
 416 samples used in training, and training time scales linearly with the number of input  
 417 samples. Our most complex model, trained on all taxa available from the NCBI SRA, has  
 418 about 1.3GB of disk size. varKode images also are tiny replacements (8.2 KB on average for  
 419 k-mer length of 7) for much larger genomic data sets (on average, 144 MB per sample  
 420 here). Downloading up to 20Mb of sequence data for over 250,000 accessions from the

421 NCBI SRA was the bottleneck, taking over 70 days. By parallelizing processing over 40  
422 cores, processing this data into varKodes was about 10 times faster, resulting in  
423 approximately 18GB of data for all of these accessions. Training a model on more than 1.3  
424 million images took about 45 hours using only 2 GPUs. Therefore, a model with the millions  
425 of species on Earth could be trained in just a few days in a dedicated server, provided that  
426 sequence data to generate varKodes can be transferred at high speeds. Although training  
427 on large datasets requires powerful GPUs and large memory, training on small datasets and  
428 querying is possible on personal computers in a few seconds to minutes. To reduce the  
429 computational resources required for training new datasets, we provide a pre-trained  
430 model from both varKodes and rfCGRs from all taxa on SRA using the huggingface hub  
431 ([https://huggingface.co/brunoasm/vit\\_large\\_patch32\\_224.NCBI\\_SRA](https://huggingface.co/brunoasm/vit_large_patch32_224.NCBI_SRA)). See Asprino et al.<sup>100</sup>  
432 for details on the data used for this model. Whenever the data become available, a model  
433 potentially trained on millions of species can easily be ported to devices without  
434 continuous internet access. Moreover, the minimal data amounts needed for identification  
435 could be generated in seconds in a portable Nanopore device. Finally, the library  
436 preparation method based on shotgun sequencing is very simple and can be automated  
437 with portable consumer devices, such as the Nanopore Voltrax. Together, these properties  
438 allow for more widely distributed applications of varKoding, such as field-laboratory  
439 environments<sup>101</sup> or proposed distributed genetic databases<sup>102</sup>.

440

## 441 **Conclusions**

442 varKoding is universal, accurate, efficient, and holds tremendous promise for documenting  
443 and discovering Earth's biodiversity. It achieves accurate identification with minimal data  
444 compared to existing next-generation sequencing methods, while maintaining universal  
445 applicability across the Tree of Life. Its modular framework relying on widely used image  
446 formats and machine learning frameworks can evolve alongside advances in sequencing  
447 technologies, bioinformatics, and machine learning, as exemplified here by the update in  
448 image representation (*varKodes* to *rfCGRs*) and neural network architecture (resnext to  
449 ViT) after initial testing. For these reasons, we expect it will contribute for the wider  
450 adoption of genomic signatures on biodiversity assessments and ecological research,



451 overcoming current challenges<sup>39</sup>. Reference data for varKoding will be increasingly  
452 available from ambitious efforts in genome sequencing<sup>103-107</sup>. However, we note that  
453 reference data for varKoding is much easier and cost-effective to obtain from low-coverage  
454 genome skims than high-quality contiguous genomes: the robustness to minimal levels of  
455 coverage a central advantage of our method. For example, our cost for a 3× skim of  
456 herbarium samples is about \$34 per sample, versus a high-quality genome which may cost  
457 tens-of-thousands of dollars each. Thus, varKoding shows tremendous promise for further  
458 automating species identification from natural history collections<sup>108-110</sup>.

459  
460 We expect that varKoding will be invaluable to the biodiversity science community in  
461 numerous ways, with many avenues remaining to be explored. One of them is the  
462 identification of samples with poor-quality and degraded DNA, such as unidentified  
463 fragmentary fossil and subfossil remains in natural history collections<sup>108,111</sup>. For example,  
464 Malpighiales samples with signs of DNA damage could be correctly identified using  
465 *varKoder* to species or genus in many cases and to family in almost every case. Future  
466 research could explore the lower limits of sample quality and sequence coverage to achieve  
467 accurate identification at different divergence levels. Moreover, a promising avenue of  
468 research is to identify the genomic features driving the success of identification based on  
469 such low sequence coverage. It is possible that the changes in repeat patterns are more  
470 important drivers of genomic evolution than currently appreciated<sup>31,51-55</sup>. Finally, we  
471 expect that new neural network architectures and forms of DNA representation will  
472 continue to be explored. One limitation of varKoding, as applied here, is the challenging  
473 identification of samples within mixed components such as lichens or environmental DNA.  
474 However, with long-read sequencing, *varKodes* and *rfCGRs* from single reads could  
475 potentially include sufficient data for that end. Moreover, mixed samples could be useful for  
476 other ends: *varKodes* could be used to classify a set of sequences based on any kind of  
477 metadata, beyond taxonomy as demonstrated by our test on the geographical origin of a  
478 soil sample.

## 479 **Author contributions**

480 BASM conceived varKodes and wrote the program *varKoder*. BASM and CCD designed the  
481 research. CCD, CA and XD designed sampling and lab methodology for the new sequence  
482 data. CCD, XD, YY, LCM, and CA collected the new sequence data. BASM and PJF collated  
483 datasets from published data. BASM, CCD, LC, YY and PJF analyzed and interpreted the data.  
484 BASM, CCD, LCM and PF prepared the figures. BASM and CCD wrote the manuscript with  
485 key contributions from LC, YY, CA and PJF. All authors approved the manuscript.

## 486 **Acknowledgments**

487 BdM was supported by the Harvard University Museum of Comparative Zoology, the  
488 Smithsonian Tropical Research Institute and the Walder Foundation. LC was supported by  
489 Harvard University and by a Stengl Wyer scholarship from the University of Texas at  
490 Austin. PF was supported by LVMH Research, and Dior Science. YY was supported by a  
491 postdoctoral fellowship from Harvard University Herbaria. CCD was supported by Harvard  
492 University, LVMH Research, Dior Science, and National Science Foundation grants DEB-  
493 1355064 and DEB-0544039. Computations were performed at the Harvard Cannon Cluster  
494 and the Field Museum Grainger Bioinformatics Center. We thank the Bauer Core Facility,  
495 and especially Claire Reardon, at Harvard University for providing technical support during  
496 the laboratory process. We thank Renata Asprino and Kylee Peterson for their assistance in  
497 obtaining the newly sequenced data under Harvard's Binding Participation Agreement. The  
498 team at Sound Solutions for Sustainable Science carefully edited early versions of our  
499 manuscript.

## 500 **Online Methods**

### 501 **Sequence data**

502 *Taxon sampling, DNA sequencing, assembly, and annotation for newly acquired genetic*  
503 *data*—The newly generated plant data used here and the methods to obtain these data are

504 described in detail in a data descriptor article<sup>100</sup>. Briefly, they included members of the  
505 large and diverse order Malpighiales<sup>34</sup>: Malpighiaceae (251 accessions representing 31  
506 genera), Elatinaceae (6 accession for 1 genus), and Chrysobalanaceae (30 accessions for 8  
507 genera). Malpighiaceae includes *Stigmaphyllon* with the most comprehensive species  
508 sampling: 10 species and 10 accessions sampled per species. All 100 *Stigmaphyllon*  
509 samples were sequenced specifically to build, validate, and test our identification models at  
510 shallower phylogenetic depths, since their taxonomy has been extensively revised by  
511 coauthor C. Anderson<sup>68,69</sup>. Each of these samples was labeled with species, genus, and  
512 family names. The focus for the remainder of the Malpighiaceae, Chrysobalanaceae, and  
513 Elatinaceae sampling was to identify a given sample to genus. In this case, among the non-  
514 *Stigmaphyllon* samples we included 3–9 species per genus. Each accession in this case was  
515 labeled with its corresponding genus and family identification. Unlike *Stigmaphyllon*, where  
516 we included multiple accessions per species, there were no additional replicates per  
517 species for our genus-level sampling. For this dataset, we used leave-one-out cross  
518 validation in all assessments, and therefore there are no train and validation sets. For  
519 additional information see Asprino et al.<sup>100</sup>.

520 *Public genomic data compilation*—To further understand the versatility of varKodes more  
521 broadly across the Tree of Life, we tested species identification using genome skim data  
522 sets from four genera of plants, animals, fungi, and a bacterial species. For each of the four  
523 organismal clades, we trained a multi-label model that included five species with at least  
524 three samples per species. This involved a plant data set from coralroot orchids (genus  
525 *Corallorhiza*)<sup>97</sup>, with five species (or varieties) with at least five samples per species, except  
526 for *C. striata* var. *vreelandii* and *C. striata* var. *striata*, for which we included six and seven  
527 samples each, respectively. The animal data consisted of a beetle data set in the genus  
528 *Bembidion*<sup>54,95</sup>, which included five species with five samples per species. The fungal  
529 dataset focused on a lichen-forming fungus in the genus *Xanthoparmelia*<sup>96</sup>. Since the  
530 *Xanthoparmelia* species were paraphyletic, we subsampled only monophyletic groups for  
531 model training. In this case, four species included three samples per species (*X.*  
532 *camtschadalis*, *X. mexicana*, *X. neocumberlandia*, and *X. coloradoensis*) and one species  
533 included five samples per species (*X. chlorochroa*). One potential confounding factor for the

534 *Xanthoparmelia* model is that *Xanthoparmelia* is a lichen-forming fungus and thus genome  
535 skim data represents a chimera of fungal and algal genomes representing both partners in  
536 this unique symbiosis. Species of the algal symbiont *Trebouxia* are flexible generalists  
537 across fungal species *Xanthoparmelia*. Since these genome skims are a mix of both algal  
538 photobiont and fungus, we hypothesize that the accuracy of our model decreased because  
539 of the more generalist nature of *Trebouxia*<sup>112</sup>. Finally, the bacterial data set included clinical  
540 isolates from *Mycobacterium tuberculosis*, the species of pathogenic bacteria that causes  
541 tuberculosis<sup>98</sup>. We included representatives of five monophyletic *M. tuberculosis* lineages  
542 (L1, L2, L3, L4.1.i1.2.1, and L4.3.i2) with seven clinical isolates per lineage. In all these  
543 cases, we labeled samples with the lowest-level taxonomic identification available (species,  
544 subspecies or isolates). For taxa with two or more samples available, 20% (with a  
545 minimum of 1) were randomly selected for the validation set, which also included all taxa  
546 represented by a single sample (therefore, absent from the training set). The remaining  
547 accessions were used in the training set. See Asprino et al.<sup>100</sup> for further information.

548 We also compiled two broad datasets from the NCBI SRA. The first consists of all 861  
549 eukaryotic families with sequenced under the Illumina platform from whole genome  
550 shotgun (WGS) libraries and up to 10 Mbp of data (download date March 7, 2023). This  
551 comprised 8,222 accessions, including families of animals (5,642 accessions, 1,426  
552 families), plants (2,705 accessions, 401 families) and fungi (1,572 accessions, 363 families).  
553 We labeled samples with family name only and included taxa with at least two associated  
554 accessions in the training set. Our validation set consisted of 20% randomly selected  
555 accessions from each family (with a minimum of one), plus all accessions in families with a  
556 single accession available (therefore not part of the training set). Only eight of the 8,222  
557 samples included yielded less than 10Mbp after sequence cleanup for varKode preparation,  
558 and all at least 100 Kbp. The second broad-scale dataset includes all taxa on NCBI SRA that  
559 could be represented by at least 3 independent accessions. In this case, we included data  
560 amounts of up to 20 Mbp, different sequencing platforms (Illumina, PacBio, Nanopore,  
561 BGISEQ) and library preparation methods (whole genome shotgun, RADseq, GBS)  
562 downloaded on January 9, 2024. For taxa with too many sequences available (such as  
563 humans, crops, disease agents, etc.), we randomly chose up to 20 accessions for each

564 combination of sequencing platform and library preparation method. The resulting dataset  
565 includes 253,820 accessions associated 28,636 taxonomic labels. In the training set,  
566 97.52% of the accessions included 10Mbp of cleaned data, with the remainder having at  
567 least 500Kbp. Accessions were labeled with all NCBI taxonomy ranks available (from infra-  
568 specific taxa to domain), the library preparation method, and the sequencing platform. The  
569 validation set, in this case, consisted of a random selection of 10% of all samples, not  
570 stratified by taxon. For additional information, see Asprino et al.<sup>100</sup>.

571  
572 Our final dataset was assembled with the aim to extend varKoder beyond taxonomic  
573 identification. We compiled a global soil metagenome eDNA dataset labeled with continent  
574 of origin from Ma et al.<sup>99</sup> We filtered out any metagenomic sample which lacked  
575 information on continent in the Ma et al. This yielded 2916 soil metagenome samples  
576 across all seven continents. We downloaded 10Mbp DNA data for each sample directly  
577 from NCBI. All code used to download and analyze these data can be found in the GitHub  
578 repository for our study ([https://www.github.com/brunoasm/varkoder\\_development](https://www.github.com/brunoasm/varkoder_development)).  
579

## 580 **varKode design and testing**

581 *Sequence data preprocessing*—Prior to the construction of images, raw reads were lightly  
582 cleaned using the following steps: identical reads were de-duplicated using *clumpify.sh* as  
583 implemented in *BBtools*<sup>84,113</sup>, adapters were removed, low-quality tails trimmed, and  
584 overlapping read pairs merged using *fastp*<sup>86</sup> with options "--detect\_adapter\_for\_pe", "--  
585 dedup", "--dup\_calc\_accuracy 1", "--disable\_quality\_filtering", "--disable\_length\_filtering", "--  
586 trim\_poly\_g", "--merge", "--include\_unmerged", . Next, we randomly selected subsets of  
587 cleaned reads with predefined data amounts, ranging from 500 kbp to 200 Mbp, with  
588 *BBtools*. These data subsets were used to generate a variety of input varKodes for a single  
589 sample and all such images were used for training (see main text and Figure 2A). Finally,  
590 we applied *dsk*<sup>85</sup> to count k-mers of a given length based on clean raw reads (i. e. k-mers  
591 are counted for each read and their frequencies are pooled across reads). *dsk* exhibits good  
592 performance with low memory requirements, which is ideal for potential applications

593 using varKodes on low-memory devices. We note that analyses for species-level public  
594 datasets have low computational requirements and were performed on an Apple MacBook  
595 with ARM processor architecture.

596 *varKode and rfCGR construction*— We designed novel images—**varKodes**—that portray  
597 relative frequencies of k-mers from low-coverage raw Illumina reads. These are similar to a  
598 frequency chaos game representation (*fCGR*) *sensu* Jeffrey<sup>53</sup>, but optimized for raw reads in  
599 which sequence orientation is unknown, and therefore canonical k-mers and their reverse  
600 complement are indistinguishable. This averaging of canonical k-mer frequencies and their  
601 reverse complements is widely used in the context of raw reads<sup>40,61,62,114,115</sup>. We call these  
602 images varKodes because they enCODE the VARIation in k-mer frequencies in a sample. We  
603 name our method **varKoding** after varKodes, but notice that it is modular and can use  
604 other kinds of DNA image representation. They are meant to represent a genomic signature  
605 by mapping k-mer identity to pixel position in an image, such that k-mers with more  
606 similar composition are closer together. Additionally, the brightness of these pixels  
607 represents the abundance of the associated k-mer, but we use ranks instead of raw  
608 frequencies to decrease the effect of overabundant and artifactual k-mers. In summary,  
609 varKodes are produced by mapping k-mer counts onto a pre-computed map of k-mers to  
610 pixels, and transforming frequency data to pixel brightness. varKode design employed t-  
611 SNE<sup>116</sup> and the python libraries *numpy*<sup>88</sup> and *pillow*<sup>117</sup>. In addition to varKodes, here we  
612 also developed a new image representation that uses the same pixel mapping as *fCGRs* but  
613 represents k-mer abundance as ranks instead of raw frequencies. We named these ranked  
614 frequency chaos game representation (*rfCGR*). Both varKodes and *fCGRs* are saved as 8-bit  
615 PNG images including labels as exif metadata.

616 *Testing k-mer length and data amount*—We employed *fastai*<sup>89</sup> for, a high-level  
617 implementation of neural networks based on *pytorch*<sup>64</sup> for training and prediction. All the  
618 model architectures we applied are image classification models available from the *timm*  
619 library<sup>90</sup>, which have been widely tested using a variety of image types. To identify the  
620 optimal training hyperparameters for our neural network, we conducted a series of tests  
621 using the species-level data set for the genus *Stigmaphyllon*. We generated varKodes for

622 each of the *Stigmaphyllon* samples. We first tested the joint effect of k-mer length and input  
623 data amount for neural network classification accuracy by selecting three samples per  
624 species as a validation set; the remaining samples were used to train neural networks using  
625 different amounts of input data across 10 randomly generated training sets. As input data  
626 for both the validation and training sets, we randomly subsampled the original sequences  
627 into fastq files containing from 500 Kb to 200 Mb (equivalent to about 1,700 to 670,000  
628 2x150bp Illumina reads). In this test, we only included samples that yielded at least 200  
629 million base pairs after cleaning. We also tested the effect of including images for all data  
630 amounts during training. For each replicate, we applied the widely used image  
631 classification neural network *resnet50* architecture<sup>118</sup> to classify varKodes and trained  
632 models for 30 epochs. We visualized the distribution of validation accuracy for each  
633 combination of input data amount and k-mer lengths to find a good balance between both.  
634 Visualizations and code applied for training and evaluation is available in our GitHub  
635 repository ([https://www.github.com/brunoasm/varkoder\\_development](https://www.github.com/brunoasm/varkoder_development)).

636 *Neural network optimization*—After identifying an appropriate k-mer length and input data  
637 used to produce varKodes (**Figure 3**), we next tested a series of neural network training  
638 conditions. We varied the neural network model complexity, choosing from seven  
639 commonly used architectures: *resnet50*<sup>118</sup>, *resnet-D*<sup>70</sup> with different depths (18, 50, 101), a  
640 wide *resnet50*<sup>70</sup>, *efficientnet-B4*<sup>119</sup>, and ResNeXt101<sup>77</sup>. We also tested the effect of the  
641 following: random initial weights vs. pretrained weights from the *timm* library<sup>90</sup>, presence  
642 or absence of lighting transforms, presence or absence of label smoothing, and presence or  
643 absence of augmentation strategies (i.e., *CutMix*<sup>76</sup> or *MixUp*<sup>75</sup>). Because these parameters  
644 may have complex interactions, we tested all combinations of architecture, pretraining,  
645 transforms, label smoothing, and augmentation, with 20 replicates for each combination of  
646 conditions. In each replicate, we randomly chose 20% of the samples for each species of  
647 *Stigmaphyllon* as validation and trained the model using the remainder for 30 epochs.  
648 Training was performed using all varKodes available for each sample (from 500kbp to  
649 200Mbp). For validation, we separately evaluated whether each varKode with a different  
650 amount of data was correctly identified. For each replicate and amount of data used to  
651 validate varKodes, we recorded the average validation accuracy across the validation set.

652 We then applied a linear model to predict the effect of all training parameters and amount  
653 of data in varKodes in the validation set on validation accuracy. Validation accuracy in this  
654 case was arc-sin transformed for linear modeling due to its bounded range of 0–1. We  
655 started from the full model containing all parameters and their interactions and reduced  
656 the model step-wise based on AIC scores (i. e. Akaike Information Criteria), as implemented  
657 in the R function `step`. Visualizations and code applied for training and evaluation is  
658 available in our GitHub repository  
659 ([https://www.github.com/brunoasm/varkoder\\_development](https://www.github.com/brunoasm/varkoder_development)).

660

661 *Testing sample number requirements*—A legitimate concern with complex neural networks  
662 is that they may require vast amounts of training data and that typical skimming data sets  
663 might be insufficient for them to be useful. We tested the robustness of our models to the  
664 effect of the number of samples per species included in training by using from one to seven  
665 samples per species as training set and the remaining as validation, with 50 replicates per  
666 number of training samples. The batch size used in training was adjusted for the cases with  
667 very few samples included, so that each training epoch included about 10 batches. We  
668 included varKodes from 1Mbp to 200Mbp in both training and validation sets. In this case,  
669 we applied the training parameters informed by our previous analyses: a *resnext101*  
670 architecture, random initial weights, *CutMix* augmentation, and label smoothing for 30  
671 epochs. We visualized the effect of the number of samples by plotting the average  
672 validation accuracy of each sample against the number of training samples used in each  
673 case. Visualizations and code applied for training and evaluation is available in our GitHub  
674 repository ([https://www.github.com/brunoasm/varkoder\\_development](https://www.github.com/brunoasm/varkoder_development)).

675

676 *Testing the effect of data quality*—Most of the cases with low accuracy corresponded to  
677 samples with low DNA yield (**Figure 3B**). We identified that DNA extraction yield was  
678 significantly correlated with two metrics of DNA quality: average insert size and variation  
679 in nucleotide composition along reads<sup>80</sup> (**Figure 4**). *varKodes* produced from these samples



680 may be visually distinct from other samples of the same species (**Figure 5**). For this reason,  
681 we further tested whether sample quality in training or validation impacted accuracy.  
682 Using both quality metrics, we identified the five lowest quality samples for each species.  
683 We next produced training sets using six randomly chosen samples per species, varying the  
684 number of low-quality samples included in training from zero to four. We included  
685 varKodes from 1Mbp to 200Mbp in both training and validation sets. We repeated this for  
686 30 replicates for each number of low-quality samples. Like our tests with varying sample  
687 numbers, we applied the following training parameters: a *resnext101* architecture, random  
688 initial weights, *CutMix* augmentation, label smoothing for 30 epochs. For the validation set,  
689 we separately recorded the accuracy for high- and low-quality samples. We then visualized  
690 the effect of inclusion of low-quality samples in the training set by observing the  
691 distribution of validation accuracies for high-quality and low-quality samples across the  
692 range of number of low-quality samples included in the training set. Visualizations and  
693 code applied for training and evaluation is available in our GitHub repository  
694 ([https://www.github.com/brunoasm/varkoder\\_development](https://www.github.com/brunoasm/varkoder_development)).

695

696 *Implementation of varKoder*—Following all the tests described above, we implemented the  
697 optimal neural network training strategies in a python program named **varKoder**.  
698 *varKoder* can process, train and query varKodes and is freely available on our GitHub:  
699 <https://github.com/brunoasm/varKoder>. Because it employs standard neural network  
700 frameworks (namely, *pytorch*<sup>64</sup>, *fastai*<sup>89</sup>, and *timm*<sup>90</sup>), any of the image classification models  
701 and training hyperparameters available now or in the future via these libraries can be  
702 easily adapted and applied to varKode classification. Moreover, we have implemented a  
703 multi-label model as the default to increase robustness to low-quality varKodes with little  
704 diagnostic information in the training set. This was done by using an asymmetric multi-  
705 label loss function<sup>82</sup> instead of the standard cross-entropy loss function used in single-label  
706 classification. Analyses used development versions of *varKoder* starting with v.0.8.0.  
707 Improvements suggested during the peer-review process are now implemented in  
708 *varKoder* v.1.1.0.

## 709 ***varKoder* evaluation and comparison to alternatives**

710 *varKoder*—To test *varKoder* performance on a complex dataset spanning multiple  
711 taxonomic levels and varying phylogenetic depths, we used the Malpighiales dataset  
712 including genera in Elatinaceae, Chrysobalanaceae and Malpighiaceae. Species of  
713 *Stigmaphyllon* (Malpighiaceae) were labeled with species, genus, and family names; all  
714 other samples were labeled with genus and family names. We tested the performance of  
715 *varKoder* in each sample with leave-one-out cross-validation. For each sample, we retained  
716 it as validation and trained a neural network using all the other samples. In preliminary  
717 assessments, we found that a ViT<sup>72</sup> architecture combined with a multi-label model  
718 sometimes led to instability in training for some datasets. For that reason, we used a two-  
719 step approach. Models first were pre-trained for 20 epochs as single-label, using the least  
720 inclusive taxonomic assignment available for each sample and a base learning rate of 0.05.  
721 Next, we trained for an additional 10 epochs using the pre-trained weights but with a much  
722 smaller learning rate (0.005) and a multi-label output. Training samples included varKodes  
723 from 500 Kbp to 200 Mbp, and we recorded validation accuracy separately for varKodes  
724 produced from each amount of data. We used an arbitrary confidence threshold of 0.7 to  
725 make predictions in the multilabel models. For validation samples, we deemed a prediction  
726 correct if only the correct taxon was predicted for each taxonomic rank (i.e., species, genus,  
727 family). We deemed a prediction incorrect if one or more predictions passed the threshold  
728 for a taxonomic rank, but none match the actual label. When predicted labels included both  
729 the correct and incorrect taxa, we deemed it ambiguous. If the output prediction included  
730 no taxon with confidence above the threshold, we considered it as inconclusive. As metrics  
731 across all samples, we used prediction and recall, averaged across all predictions. We  
732 visualized the fraction of correct, incorrect, ambiguous, and inconclusive samples for each  
733 taxonomic rank and each amount of data used to produce varKodes. The code to reproduce  
734 training conditions and evaluation tests is available on GitHub  
735 ([https://www.github.com/brunoasm/varkoder\\_development](https://www.github.com/brunoasm/varkoder_development)).

736 To test the joint effect of neural network architecture and image representation method,  
737 we applied this cross-validation approach to all combinations of three image

738 representations and four neural network architectures. The architectures tested included:  
739 (1) *ResNeXt101*<sup>77</sup>, the optimal convolutional neural network architecture in our initial tests,  
740 (2) *ViT*<sup>72</sup>, a transformer-based architecture that became available after our initial testing,  
741 (3) a neural network with two convolutional layers processing vectorized k-mer counts,  
742 following Fiannaca et al<sup>44</sup> and (4) a multi-layer perceptron formed by a series of fully  
743 connected layers as specified in Millán Arias et al<sup>42</sup>. The two latter have been previously  
744 employed for *fCGR* data. The three representations tested include *varKodes* and *rfCGRs* as  
745 developed here, and *fCGRs* as estimated by iDeLUCS<sup>93</sup>. In the latter case, we used iDeLUCS  
746 functions to produce *fCGRs* as 2D python arrays of k-mer counts. Next, we rescaled these  
747 counts to the range of 0–255 and rounded them to the nearest integer. These arrays were  
748 then saved as 8-bit png images. In all tests, we employed the same data augmentation  
749 methods and loss function as for *varKodes* and *rfCGRs*. All code used in *varKoder* analyses is  
750 available on GitHub ([https://www.github.com/brunoasm/varkoder\\_development](https://www.github.com/brunoasm/varkoder_development)).

751 *Skmer*—To compare *varKoder* with alternative methods, we used fastq files cleaned and  
752 subsampled by *varKoder* as input files to *Skmer*. In this case, we also used leave-one-out  
753 cross-validation to evaluate performance. For each amount of input data (500Kbp to  
754 200Mbp), we cycled through all samples, constructing a *Skmer* database with the "*skmer*  
755 *reference*" command and including all samples but one and default settings. We then used  
756 the "*skmer query*" command with default settings on the sample left out and deemed the  
757 identification as correct if the sample in the reference database with closest estimated  
758 genetic distance had the correct taxon label. Because *Skmer* could always query a sample  
759 and there is no objective criterion to consider matches beyond the best match, the output  
760 predictions can only be correct or incorrect, but not inconclusive or ambiguous. We  
761 visualized the results similarly as we did with *varKoder*. The code to reproduce *Skmer*  
762 analyses is available on GitHub  
763 ([https://www.github.com/brunoasm/varkoder\\_development](https://www.github.com/brunoasm/varkoder_development)).

764 *Conventional plant barcodes* —For conventional barcodes, we applied standard BLAST- and  
765 phylogeny-based methods, which do not involve machine learning. To infer phylogenies  
766 from our genome skim data (Figure 1), we applied the *PhyloHerb* bioinformatic pipeline<sup>120</sup>,

767 which has been applied recently to a taxa ranging from algae to flowering plants<sup>121-123</sup>.  
768 Briefly, this pipeline works as follows: for plastid loci, *PhyloHerb* maps raw short reads to a  
769 database of land plant plastid genomes. Mapped reads are then assembled into scaffolds  
770 using *SPAdes*<sup>124</sup> and plastid loci are identified using nucleotide BLAST searches with a  
771 default e-value threshold of 1e-40. *PhyloHerb* then outputs orthologous plastid genes into  
772 individual FASTA files, which are fed directly into MAFFT v7.407<sup>125</sup> for alignment.  
773 Alignments are then concatenated into a super matrix using the 'conc' function within the  
774 *PhyloHerb* package. Phylogenies for both individual locus and the concatenated alignment  
775 were inferred with IQTREE v2.0.6 using the GTR+GAMMA model with 1000 ultrafast  
776 bootstrap replicates<sup>126</sup>.

777 To recover the conventional plant barcodes, *rbcl*, *matK*, *trnL-F*, *ndhF*, and ITS, from our  
778 Malpighiales genome skim data, we applied *GetOrganelle* v1.7.7.0<sup>127</sup> and *PhyloHerb*  
779 v1.1.1<sup>120</sup> to automatically assemble and extract these DNA markers, respectively. Briefly,  
780 the complete or subsampled genome skim data were first assembled into plastid genomes  
781 or nuclear ribosomal regions using *GetOrganelle* with its default settings. Next, *PhyloHerb*  
782 was applied to extract the relevant barcode genes using its built-in BLAST database. To test  
783 whether these traditional barcodes provided accurate identification to species, genus, and  
784 family, we ran an all-by-all BLASTn analysis for each individual gene across the same data  
785 subsampling schemes as *Skmer* and *varKoder*. BLAST targets were always drawn from  
786 assemblies using all the data available for each specimen, whereas queries included  
787 assemblies from input data amounts varying from 500 Kbp to 200 Mbp. Within each BLAST  
788 analysis for each one of the Malpighiales accessions, we deemed an identification to be  
789 correct if the best non-self BLAST hit came from the same taxon, and incorrect otherwise.  
790 We deemed it inconclusive if the locus could not be assembled for that amount of data. For  
791 concatenated barcodes, we produced a phylogenetic tree for each amount of data and  
792 deemed an identification to be correct if the sample with lowest patristic distance came  
793 from the same taxon. We deemed it to be inconclusive when none of the genes in the  
794 concatenated dataset could be assembled for a sample. We visualized results similarly to  
795 *varKoder*, separately for each conventional barcoding gene and for the concatenated

796 dataset. The code to reproduce conventional barcode analyses is available on GitHub  
797 ([https://www.github.com/brunoasm/varkoder\\_development](https://www.github.com/brunoasm/varkoder_development)).

798 *iDeLUCS*—To evaluate the performance of *varKoder* with another deep learning based  
799 sequence classifier, we applied the sequences assembled from the *PhyloHerb* pipeline to  
800 *iDeLUCS*<sup>93</sup>. We first used concatenated sequences of five traditional plant barcodes (*rbcL*,  
801 *matK*, *trnL-F*, *ndhF*, and ITS) assembled from input reads varying from 500 Kbp to 200  
802 Mbp. *iDeLUCS* was run with k-mer length of 6, 100 training epochs, 100 data augmentations  
803 per sequence, and the SGD algorithm for neural network optimization. Unlike *varKoder*,  
804 *iDeLUCS* does unsupervised clustering and therefore does not use labels during training.  
805 Instead, all input accessions were set to be clustered into 10 groups (equal to the total  
806 number of species) and the accuracy was evaluated with the *cluster\_acc* function  
807 implemented in *iDeLUCS*. We also applied the entire plastid genome and the nuclear  
808 ribosomal sequence assemblies (ETS+18S+ITS1+5.8S+ITS2+28S) in *iDeLUCS* with the same  
809 parameters to evaluate the impact of input data quality.

## 810 **Application in diverse taxa**

811 *Species-level identification in plants, animals, fungi, and bacteria*— For all four test cases  
812 (*Corallorhiza*, *Bembidion*, *Xanthoparmelia*, and *Mycobacterium tuberculosis*), we applied  
813 default *varKoder* v.0.8.0 parameters for generating *rfCGR* images, training each model, and  
814 testing the accuracy of the trained model using the ‘query’ function. In all cases, we  
815 included all the available data for each training or validation sample. To test if trained  
816 models accurately predicted species identity, we queried them using extra genome skim  
817 samples not used for training but from the same species included in the model. We also  
818 tested genome skim test samples of species within the same genus *not* used in model  
819 training. As in the case of Malpighiales, we set the threshold to make a prediction equal to  
820 0.7 and used the same criteria to consider a prediction correct, incorrect, inconclusive, or  
821 ambiguous. We separately evaluated results for taxa with representatives included in the  
822 training set and taxa used only as queries, without conspecific samples in the training set.  
823 The code to reproduce these analyses is available on GitHub  
824 ([https://www.github.com/brunoasm/varkoder\\_development](https://www.github.com/brunoasm/varkoder_development)).

825

826 *All eukaryotic families data set from SRA*—Each accession was labeled with its family  
827 identification obtained from NCBI. Because of the larger size of this dataset, a leave-one-out  
828 cross-validation approach would have been intractable. Therefore, we randomly selected  
829 80% of the samples in each family as the training set and used the remainder for validation.  
830 Similarly to Malpighiales, we used a two-step training method by pre-training as a single-  
831 label model and finalizing with a multi-label model. Pre-training was done with a learning  
832 rate of 0.1 and a batch size of 300 for 30 epochs. Final training was done with the same  
833 batch size but a smaller base learning rate of 0.01 in 5 epochs with frozen body weights and  
834 three epochs with unfrozen weights. The code to reproduce these analyses is available on  
835 GitHub ([https://www.github.com/brunoasm/varkoder\\_development](https://www.github.com/brunoasm/varkoder_development)).

836

837 *All taxa from SRA*— For each accession, we created *rfCGRs* from 500Kbp to 10Mbp of data.  
838 Each accession was labeled with all the taxa in its taxonomic tree (that is, from infra-  
839 specific taxa to domains of life), as well as library strategy (RAD, GBS or WGS) and  
840 sequencing platform (Illumina, PACBIO, Nanopore or BGISEQ). We randomly selected 10%  
841 of the samples as validation set, and eliminated from validation samples all labels absent  
842 from the training set. We used a two-step training method. First, we pre-trained using a  
843 single-label strategy, using as labels the concatenation of library strategy, sequencing  
844 platform, kingdom, family and genus. For pretraining, we used a learning rate of 0.1, a  
845 batch size of 500 and 30 epochs. We then used the weights of this pre-trained model as  
846 starting weights for a multi-label model including all labels. We trained the model for  
847 additional 50 epochs with unfrozen body weights and 10 epochs with frozen weights,  
848 learning rate of 0.05 and batch size of 600. The code to reproduce these analyses is  
849 available on GitHub ([https://www.github.com/brunoasm/varkoder\\_development](https://www.github.com/brunoasm/varkoder_development)).

850

851 *Environmental metagenome global identification*—The downloaded soil metagenomes from  
852 Ma et al.<sup>99</sup> were labeled by source continent. Similarly to the eukaryotic family data set  
853 from SRA, we randomly selected 80% of the samples as the training set and used the  
854 remaining 20% as the validation set. We used a two-step training method by pre-training  
855 as a single-label model and finalizing with a multi-label model. Pre-training was done with

856 a learning rate of 0.1 and a batch size of 64 for 30 epochs. Final training was done with the  
857 same batch size but a smaller base learning rate of 0.01 in 5 epochs with frozen body  
858 weights and three epochs with unfrozen weights. The code to reproduce all these analyses  
859 is available on GitHub ([https://www.github.com/brunoasm/varkoder\\_development](https://www.github.com/brunoasm/varkoder_development)).

## 860 **References**

- 861 1. Hebert, P. D. N., Ratnasingham, S. & de Waard, J. R. Barcoding animal life: cytochrome c  
862 oxidase subunit 1 divergences among closely related species. *Proc. R. Soc. Lond. B Biol. Sci.*  
863 270, S96–S99 (2003).
- 864 2. Kress, W. J. Plant DNA barcodes: Applications today and in the future. *J. Syst. Evol.* 55,  
865 291–307 (2017).
- 866 3. Ratnasingham, S. & Hebert, P. D. N. BOLD: The Barcode of Life Data System  
867 (www.barcodinglife.org). *Mol. Ecol. Notes* 7, 355–364 (2007).
- 868 4. Taberlet, P., Coissac, E., Pompanon, F., Brochmann, C. & Willerslev, E. Towards next-  
869 generation biodiversity assessment using DNA metabarcoding. *Mol. Ecol.* 21, 2045–2050  
870 (2012).
- 871 5. Seifert, K. A. Progress towards DNA barcoding of fungi. *Mol. Ecol. Resour.* 9 Suppl s1, 83–  
872 89 (2009).
- 873 6. Sharkey, M. J. et al. Minimalist revision and description of 403 new species in 11  
874 subfamilies of Costa Rican braconid parasitoid wasps, including host records for 219  
875 species. *ZooKeys* 1013, 1–665 (2021).
- 876 7. Lahaye, R. et al. DNA barcoding the floras of biodiversity hotspots. *Proc. Natl. Acad. Sci. U.*  
877 *S. A.* 0709936105 (2008) doi:10.1073/pnas.0709936105.
- 878 8. Kuzmina, M. L. et al. Using herbarium-derived DNAs to assemble a large-scale DNA  
879 barcode library for the vascular plants of Canada. *Appl. Plant Sci.* 5, apps.1700079 (2017).
- 880 9. Muñoz-Rodríguez, P. et al. A taxonomic monograph of *Ipomoea* integrated across  
881 phylogenetic scales. *Nat. Plants* 5, 1136–1144 (2019).
- 882 10. Hebert, P. D., Penton, E. H., Burns, J. M., Janzen, D. H. & Hallwachs, W. Ten species in one:  
883 DNA barcoding reveals cryptic species in the neotropical skipper butterfly *Astraptes*  
884 *fulgerator*. *Proc. Natl. Acad. Sci. U. S. A.* 101, 14812–14817 (2004).
- 885  
886  
887  
888  
889  
890  
891  
892  
893  
894

- 895 11. Zeale, M. R., Butlin, R. K., Barker, G. L., Lees, D. C. & Jones, G. Taxon-specific PCR for DNA  
896 barcoding arthropod prey in bat faeces. *Mol. Ecol. Resour.* 11, 236–244 (2011).  
897
- 898 12. Nitta, J. H., Meyer, J., Taputuarai, R. & Davis, C. C. Life cycle matters: DNA barcoding  
899 reveals contrasting community structure between fern sporophytes and gametophytes.  
900 *Ecol. Monogr.* 87, 278–296 (2016).  
901
- 902 13. Kress, W. J. et al. Plant DNA barcodes and a community phylogeny of a tropical forest  
903 dynamics plot in Panama. *Proc. Natl. Acad. Sci. U. S. A.* 106, 18621–18626 (2009).  
904
- 905 14. Willis, C. G., Franzone, B. F., Xi, Z. & Davis, C. C. The establishment of Central American  
906 migratory corridors and the biogeographic origins of seasonally dry tropical forests in  
907 Mexico. *Front. Genet.* 5, 433 (2014).  
908
- 909 15. Willerslev, E. et al. Ancient biomolecules from deep ice cores reveal a forested Southern  
910 Greenland. *Science* 317, 111–114 (2007).  
911
- 912 16. Crump, S. E. et al. Ancient plant DNA reveals High Arctic greening during the Last  
913 Interglacial. *Proc. Natl. Acad. Sci. U. S. A.* 118, e2019069118 (2021).  
914
- 915 17. Kjær, K. H. et al. A 2-million-year-old ecosystem in Greenland uncovered by  
916 environmental DNA. *Nature* 612, 283–291 (2022).  
917
- 918 18. Fierer, N. et al. Forensic identification using skin bacterial communities. *Proc. Natl.*  
919 *Acad. Sci.* 107, 6477–81 (2010).  
920
- 921 19. Rollo, F., Ubaldi, M., Ermini, L. & Marota, I. Ötzi's last meals: DNA analysis of the  
922 intestinal content of the Neolithic glacier mummy from the Alps. *Proc. Natl. Acad. Sci. U. S.*  
923 *A.* 99, 12594–12599 (2002).  
924
- 925 20. Yu, J. et al. Progress in the use of DNA barcodes in the identification and classification of  
926 medicinal plants. *Ecotoxicol. Environ. Saf.* 208, 111691 (2021).  
927
- 928 21. Ashfaq, M. & Hebert, P. D. N. DNA barcodes for bio-surveillance: regulated and  
929 economically important arthropod plant pests. *Genome* 59, 933–945 (2016).  
930
- 931 22. Eaton, M. J. et al. Barcoding bushmeat: molecular identification of Central African and  
932 South American harvested vertebrates. *Conserv. Genet.* 11, 1389–1404 (2010).  
933
- 934 23. Liu, J. et al. Integrating a comprehensive DNA barcode reference library with a global  
935 map of yews (*Taxus L.*) for forensic identification. *Mol. Ecol. Resour.* 18, 1115–1131 (2018).  
936
- 937 24. Ogden, R., Dawnay, N. & McEwing, R. Wildlife DNA forensics—bridging the gap between  
938 conservation genetics and law enforcement. *Endanger. Species Res.* 9, 179–195 (2009).  
939



- 940 25. Williamson, J. et al. Exposing the illegal trade in cycad species (Cycadophyta:  
941 Encephalartos) at two traditional medicine markets in South Africa using DNA barcoding.  
942 *Genome* 59, 771–781 (2016).  
943
- 944 26. Costa, F. O. & Carvalho, G. R. The Barcode of Life Initiative: synopsis and prospective  
945 societal impacts of DNA barcoding of Fish. *Genomics Soc. Policy* 3, 29 (2007).  
946
- 947 27. Gao, Z., Liu, Y., Wang, X., Wei, X. & Han, J. DNA mini-barcoding: a derived barcoding  
948 method for herbal molecular identification. *Front. Plant Sci.* 10, (2019).  
949
- 950 28. Molina, J. et al. Possible loss of the chloroplast genome in the parasitic flowering plant  
951 *Rafflesia lagascae* (Rafflesiaceae). *Mol. Biol. Evol.* 31, 793–803 (2014).  
952
- 953 29. Cai, L. et al. Deeply altered genome architecture in the endoparasitic flowering plant  
954 *Sapria himalayana* Griff. (Rafflesiaceae). *Curr. Biol.* 31, 1002–1011.e9 (2021).  
955
- 956 30. Richardson, J. E., Pennington, R. T., Pennington, T. D. & Hollingsworth, P. M. Rapid  
957 diversification of a species-rich genus of neotropical rain forest trees. *Science* 293, 2242–  
958 2245 (2001).  
959
- 960 31. Wang, J., Luo, J., Ma, Y.-Z., Mao, X.-X. & Liu, J.-Q. Nuclear simple sequence repeat markers  
961 are superior to DNA barcodes for identification of closely related *Rhododendron* species on  
962 the same mountain. *J. Syst. Evol.* 57, 278–286 (2019).  
963
- 964 32. Su, X., Wu, G., Li, L. & Liu, J. Species delimitation in plants using the Qinghai–Tibet  
965 Plateau endemic *Orinus* (Poaceae: Tridentinae) as an example. *Ann. Bot.* 116, 35–48  
966 (2015).  
967
- 968 33. Lu, Z. et al. Species delimitation and hybridization history of a hazel species complex.  
969 *Ann. Bot.* 127, 875–886 (2021).  
970
- 971 34. Cai, L. et al. The perfect storm: gene tree estimation error, incomplete lineage sorting,  
972 and ancient gene flow explain the most recalcitrant ancient angiosperm clade, Malpighiales.  
973 *Syst. Biol.* 70, 491–507 (2021).  
974
- 975 35. Clarke, L. J., Soubrier, J., Weyrich, L. S. & Cooper, A. Environmental metabarcodes for  
976 insects: in silico PCR reveals potential for taxonomic bias. *Mol. Ecol. Resour.* 14, 1160–1170  
977 (2014).  
978
- 979 36. Song, H., Buhay, J. E., Whiting, M. F. & Crandall, K. A. Many species in one: DNA  
980 barcoding overestimates the number of species when nuclear mitochondrial pseudogenes  
981 are coamplified. *Proc. Natl. Acad. Sci. U. S. A.* 105, 13486–13491 (2008).  
982
- 983 37. Xiong, H. et al. Species tree estimation and the impact of gene loss following whole-  
984 genome duplication. *Syst. Biol.* 71, 1348–1361 (2022).  
985

- 986 38. Straub, S. C. K. et al. Navigating the tip of the genomic iceberg: Next-generation  
987 sequencing for plant systematics. *Am. J. Bot.* 99, 349–364 (2012).  
988
- 989 39. Bohmann, K., Mirarab, S., Bafna, V. & Gilbert, M. T. P. Beyond DNA barcoding: The  
990 unrealised potential of genome skim data in sample identification. *Mol. Ecol.* 1–14 (2020)  
991 doi:10.1111/mec.15507.  
992
- 993 40. Sarmashghi, S., Bohmann, K., P. Gilbert, M. T., Bafna, V. & Mirarab, S. Skmer: assembly-  
994 free and alignment-free sample identification using genome skims. *Genome Biol.* 20, 34  
995 (2019).  
996
- 997 41. Borowiec, M. L. et al. Deep learning as a tool for ecology and evolution. *Methods Ecol.*  
998 *Evol.* 13, 1640–1660 (2022).  
999
- 1000 42. Arias, P. M., Alipour, F., Hill, K. A. & Kari, L. DeLUCS: Deep learning for unsupervised  
1001 clustering of DNA sequences. *PLOS ONE* 17, e0261531 (2022).  
1002
- 1003 43. Kari, L. et al. Mapping the space of genomic signatures. *PLOS ONE* 10, e0119815 (2015).  
1004
- 1005 44. Fiannaca, A. et al. Deep learning models for bacteria taxonomic classification of  
1006 metagenomic data. *BMC Bioinformatics* 19, (2018).  
1007
- 1008 45. Linard, B., Swenson, K. & Pardi, F. Rapid alignment-free phylogenetic identification of  
1009 metagenomic sequences. *Bioinformatics* (2019) doi:10.1093/bioinformatics/btz068.  
1010
- 1011 46. Desai, H. P., Parameshwaran, A. P., Sunderraman, R. & Weeks, M. Comparative Study  
1012 Using Neural Networks for 16S Ribosomal Gene Classification. *J. Comput. Biol.* 27, 248–258  
1013 (2020).  
1014
- 1015 47. Shang, J. & Sun, Y. CHEER: HierarCHical taxonomic classification for viral mEtagEnomic  
1016 data via deep leaRning. *Methods* 189, 95–103 (2021).  
1017
- 1018 48. Arias, P. M. et al. BarcodeBERT: Transformers for Biodiversity Analysis. Preprint at  
1019 <http://arxiv.org/abs/2311.02401> (2023).  
1020
- 1021 49. Badirli, S., Akata, Z., Mohler, G., Picard, C. & Dundar, M. Fine-Grained Zero-Shot Learning  
1022 with DNA as Side Information. Preprint at <http://arxiv.org/abs/2109.14133> (2021).  
1023
- 1024 50. Lecun, Y., Bengio, Y. & Hinton, G. Deep learning. *Nature* 521, 436–444 (2015).  
1025
- 1026 51. Cong, Y., Ye, X., Mei, Y., He, K. & Li, F. Transposons and non-coding regions drive the  
1027 intrafamily differences of genome size in insects. *iScience* 25, 104873 (2022).  
1028
- 1029 52. Heckenhauer, J. et al. Genome size evolution in the diverse insect order Trichoptera.  
1030 *GigaScience* 11, 1–19 (2022).  
1031

- 1032 53. Schley, R. J. et al. The ecology of palm genomes: repeat-associated genome size  
1033 expansion is constrained by aridity. *New Phytol.* 433–446 (2022) doi:10.1111/nph.18323.  
1034
- 1035 54. Sproul, J. S., Barton, L. M. & Maddison, D. R. Repetitive DNA profiles Reveal Evidence of  
1036 Rapid Genome Evolution and Reflect Species Boundaries in Ground Beetles. *Syst. Biol.* 0, 1–  
1037 12 (2020).  
1038
- 1039 55. de Medeiros, B. A. S. & Farrell, B. D. Whole-genome amplification in double-digest  
1040 RADseq results in adequate libraries but fewer sequenced loci. *PeerJ* 6, e5089 (2018).  
1041
- 1042 56. Jeffrey, H. J. Chaos game representation of gene structure. *Nucleic Acids Res.* 18, 2163–  
1043 2170 (1990).  
1044
- 1045 57. Deschavanne, P. J., Giron, A., Vilain, J., Fagot, G. & Fertil, B. Genomic signature:  
1046 characterization and classification of species assessed by chaos game representation of  
1047 sequences. *Mol. Biol. Evol.* 16, 1391–1399 (1999).  
1048
- 1049 58. de la Fuente, R., Díaz-Villanueva, W., Arnau, V. & Moya, A. Genomic Signature in  
1050 Evolutionary Biology: A Review. *Biology* 12, 322 (2023).  
1051
- 1052 59. Avila Cartes, J., Anand, S., Ciccolella, S., Bonizzoni, P. & Della Vedova, G. Accurate and fast  
1053 clade assignment via deep learning and frequency chaos game representation. *GigaScience*  
1054 12, giac119 (2023).  
1055
- 1056 60. Solis-Reyes, S., Avino, M., Poon, A. & Kari, L. An open-source k-mer based machine  
1057 learning tool for fast and accurate subtyping of HIV-1 genomes. *PLOS ONE* 13, e0206409  
1058 (2018).  
1059
- 1060 61. Kislyuk, A., Bhatnagar, S., Dushoff, J. & Weitz, J. S. Unsupervised statistical clustering of  
1061 environmental shotgun sequences. *BMC Bioinformatics* 10, 316 (2009).  
1062
- 1063 62. Arias, P. M. et al. Environment and taxonomy shape the genomic signature of  
1064 prokaryotic extremophiles. *Sci. Rep.* 13, 16105 (2023).  
1065
- 1066 63. Murad, T., Ali, S., Khan, I. & Patterson, M. Spike2CGR: an efficient method for spike  
1067 sequence classification using chaos game representation. *Mach. Learn.* 112, 3633–3658  
1068 (2023).  
1069
- 1070 64. Paszke, A. et al. PyTorch: An Imperative Style, High-Performance Deep Learning  
1071 Library. in *Advances in Neural Information Processing Systems* 32 8024–8035 (Curran  
1072 Associates, Inc., 2019).  
1073
- 1074 65. Davis, C. C. & Anderson, W. R. A complete generic phylogeny of Malpighiaceae inferred  
1075 from nucleotide sequence data and morphology. *Am. J. Bot.* 97, 2031–2048 (2010).  
1076

- 1077 66. Cai, L. et al. Phylogeny of Elatinaceae and the tropical Gondwanan origin of the  
1078 Centropilaceae (Malpighiaceae, Elatinaceae) clade. PLOS ONE 11, e0161881 (2016).  
1079
- 1080 67. Davis, C. C., Anderson, W. R. & Donoghue, M. J. Phylogeny of Malpighiaceae: evidence  
1081 from chloroplast *ndhF* and *trnL-F* nucleotide sequences. *Am. J. Bot.* 88, 1830–1846 (2001).  
1082
- 1083 68. Anderson, C. Revision of *Ryssopterys* and transfer to *Stigmaphyllon* (Malpighiaceae).  
1084 *Blumea* 56, 73–104 (2011).  
1085
- 1086 69. Anderson, C. Monograph of *Stigmaphyllon* (Malpighiaceae). *Syst. Bot. Monogr.* 51, 1–  
1087 313 (1997).  
1088
- 1089 70. He, T. et al. Bag of Tricks for Image Classification with Convolutional Neural Networks.  
1090 Preprint at <http://arxiv.org/abs/1812.01187> (2018).  
1091
- 1092 71. Vaswani, A. et al. Attention Is All You Need. Preprint at  
1093 <https://doi.org/10.48550/arXiv.1706.03762> (2017).  
1094
- 1095 72. Dosovitskiy, A. et al. An Image is Worth 16x16 Words: Transformers for Image  
1096 Recognition at Scale. (2021).  
1097
- 1098 73. Szegedy, C., Vanhoucke, V., Ioffe, S., Shlens, J. & Wojna, Z. Rethinking the Inception  
1099 Architecture for Computer Vision. in 2016 IEEE Conference on Computer Vision and  
1100 Pattern Recognition (CVPR) 2818–2826 (2016). doi:10.1109/CVPR.2016.308.  
1101
- 1102 74. Smith, L. N. A disciplined approach to neural network hyper-parameters: Part 1 --  
1103 learning rate, batch size, momentum, and weight decay. Preprint at  
1104 <http://arxiv.org/abs/1803.09820> (2018).  
1105
- 1106 75. Zhang, H., Cisse, M., Dauphin, Y. N. & Lopez-Paz, D. mixup: Beyond Empirical Risk  
1107 Minimization. Preprint at <http://arxiv.org/abs/1710.09412> (2018).  
1108
- 1109 76. Yun, S. et al. CutMix: Regularization Strategy to Train Strong Classifiers with Localizable  
1110 Features. Preprint at <https://doi.org/10.48550/arXiv.1905.04899> (2019).  
1111
- 1112 77. Xie, S., Girshick, R., Dollár, P., Tu, Z. & He, K. Aggregated Residual Transformations for  
1113 Deep Neural Networks. Preprint at <https://doi.org/10.48550/arXiv.1611.05431> (2017).  
1114
- 1115 78. Goodfellow, I., Bengio, Y. & Courville, A. *Deep Learning*. (MIT Press, 2016).  
1116
- 1117 79. Christin, S., Hervet, É. & Lecomte, N. Applications for deep learning in ecology. *Methods*  
1118 *Ecol. Evol.* 10, 1632–1644 (2019).  
1119
- 1120 80. Weiß, C. L. et al. Temporal patterns of damage and decay kinetics of DNA retrieved from  
1121 plant herbarium specimens. *R. Soc. Open Sci.* 3, 160239 (2016).  
1122

- 1123 81. Rachtman, E., Balaban, M., Bafna, V. & Mirarab, S. The impact of contaminants on the  
1124 accuracy of genome skimming and the effectiveness of exclusion read filters. *Mol. Ecol.*  
1125 *Resour.* 20, 649–661 (2020).  
1126
- 1127 82. Ben-Baruch, E. et al. Asymmetric Loss For Multi-Label Classification. Preprint at  
1128 <http://arxiv.org/abs/2009.14119> (2021).  
1129
- 1130 83. Bushnell, B. *BBMap*. (2022).  
1131
- 1132 84. Bushnell, B., Rood, J. & Singer, E. *BBMerge* – Accurate paired shotgun read merging via  
1133 overlap. *PLOS ONE* 12, e0185056 (2017).  
1134
- 1135 85. Rizk, G., Lavenier, D. & Chikhi, R. *DSK*: k-mer counting with very low memory usage.  
1136 *Bioinformatics* 29, 652–653 (2013).  
1137
- 1138 86. Chen, S., Zhou, Y., Chen, Y. & Gu, J. *fastp*: an ultra-fast all-in-one FASTQ preprocessor.  
1139 *Bioinformatics* 34, i884–i890 (2018).  
1140
- 1141 87. Tange, O. *GNU Parallel 2018*. (Ole Tange, 2018). doi:10.5281/zenodo.1146014.  
1142
- 1143 88. Harris, C. R. et al. Array programming with NumPy. *Nature* 585, 357–362 (2020).  
1144
- 1145 89. Howard, J. & Gugger, S. *Fastai*: A Layered API for Deep Learning. *Information* 11, 108  
1146 (2020).  
1147
- 1148 90. Wightman, R. *PyTorch Image Models*. GitHub repository (2019)  
1149 doi:10.5281/zenodo.4414861.  
1150
- 1151 91. Pellicer, J. & Leitch, I. J. The Plant DNA C-values database (release 7.1): an updated  
1152 online repository of plant genome size data for comparative studies. *New Phytol.* 226, 301–  
1153 305 (2020).  
1154
- 1155 92. Fiannaca, A., La Rosa, M., Rizzo, R. & Urso, A. Analysis of DNA Barcode Sequences Using  
1156 Neural Gas and Spectral Representation. in *Engineering Applications of Neural Networks*  
1157 (eds. Iliadis, L., Pappadopoulos, H. & Jayne, C.) 212–221 (Springer, Heidelberg, 2013).  
1158
- 1159 93. Millan Arias, P., Hill, K. A. & Kari, L. *i DeLUCS*: a deep learning interactive tool for  
1160 alignment-free clustering of DNA sequences. *Bioinformatics* 39, btad508 (2023).  
1161
- 1162 94. D'Ercole, J., Prosser, S. W. J. & Hebert, P. D. N. A SMRT approach for targeted amplicon  
1163 sequencing of museum specimens (Lepidoptera)—patterns of nucleotide misincorporation.  
1164 *PeerJ* 9, e10420 (2021).  
1165
- 1166 95. Sproul, J. S. & Maddison, D. R. Cryptic species in the mountaintops: species delimitation  
1167 and taxonomy of the *Bembidion breve* species group (Coleoptera: Carabidae) aided by

- 1168 genomic architecture of a century-old type specimen. *Zool. J. Linn. Soc.* 183, 556–583  
1169 (2018).  
1170
- 1171 96. Keuler, R. et al. Interpreting phylogenetic conflict: hybridization in the most speciose  
1172 genus of lichen-forming fungi. *Mol. Phylogenet. Evol.* 174, 107543 (2022).  
1173
- 1174 97. Barrett, C. F., Wicke, S. & Sass, C. Dense infraspecific sampling reveals rapid and  
1175 independent trajectories of plastome degradation in a heterotrophic orchid complex. *New*  
1176 *Phytol.* 218, 1192–1204 (2018).  
1177
- 1178 98. Freschi, L. et al. Population structure, biogeography and transmissibility of  
1179 *Mycobacterium tuberculosis*. *Nat. Commun.* 12, 6099 (2021).  
1180
- 1181 99. Ma, B. et al. A genomic catalogue of soil microbiomes boosts mining of biodiversity and  
1182 genetic resources. *Nat. Commun.* 14, 7318 (2023).  
1183
- 1184 100. Asprino, R. et al. A dataset for benchmarking molecular identification tools based on  
1185 genome skimming. Preprint at <https://doi.org/10.32942/X2DW6K> (2024).  
1186
- 1187 101. Pomerantz, A. et al. Rapid in situ identification of biological specimens via DNA  
1188 amplicon sequencing using miniaturized laboratory equipment. *Nat. Protoc.* 17, 1415–1443  
1189 (2022).  
1190
- 1191 102. Kimura, L. T. et al. Amazon Biobank: a collaborative genetic database for bioeconomy  
1192 development. *Funct. Integr. Genomics* 23, 101 (2023).  
1193
- 1194 103. Lewin, H. A. et al. The Earth BioGenome Project 2020: starting the clock. *Proc. Natl.*  
1195 *Acad. Sci. U. S. A.* 119, e2115635118 (2022).  
1196
- 1197 104. Ebenezer, T. E. et al. Africa: sequence 100,000 species to safeguard biodiversity.  
1198 *Nature* 603, 388–392 (2022).  
1199
- 1200 105. Cheng, S. et al. 10KP: A phylodiverse genome sequencing plan. *GigaScience* 7, giy013  
1201 (2018).  
1202
- 1203 106. Staff, E. A reference standard for genome biology. *Nat. Biotechnol.* 36, 1121–1121  
1204 (2018).  
1205
- 1206 107. i5K Consortium. The i5K Initiative: Advancing Arthropod Genomics for Knowledge,  
1207 Human Health, Agriculture, and the Environment. *J. Hered.* 104, 595–600 (2013).  
1208
- 1209 108. Davis, C. C. The herbarium of the future. *Trends Ecol. Evol.* (2022)  
1210 doi:10.1016/j.tree.2022.11.015.  
1211
- 1212 109. Davis, C. C. Collections are truly priceless. *Science* 383, 1035–1035 (2024).  
1213

- 1214 110. Davis, C. C., Sessa, E. B., Paton, A., Antonelli, A. & Teisher, J. The destructive sampling  
1215 conundrum and guidelines for effective and ethical sampling of herbaria. *EcoEvoRxiv*  
1216 (2024) doi:10.32942/X2C603.  
1217
- 1218 111. Card, D. C., Shapiro, B., Giribet, G., Moritz, C. & Edwards, S. V. Museum genomics. *Annu.*  
1219 *Rev. Genet.* 55, 633–659 (2021).  
1220
- 1221 112. Leavitt, S. D. et al. Fungal specificity and selectivity for algae play a major role in  
1222 determining lichen partnerships across diverse ecogeographic regions in the lichen-  
1223 forming family Parmeliaceae (Ascomycota). *Mol. Ecol.* 24, 3779–3797 (2015).  
1224
- 1225 113. Bushnell, B. BBtools v.37.61. (2017).  
1226
- 1227 114. Nissen, J. N. et al. Improved metagenome binning and assembly using deep variational  
1228 autoencoders. *Nat. Biotechnol.* 39, 555–560 (2021).  
1229
- 1230 115. Vurture, G. W. et al. GenomeScope: fast reference-free genome profiling from short  
1231 reads. *Bioinformatics* 33, 2202–2204 (2017).  
1232
- 1233 116. Maaten, L. van der & Hinton, G. Visualizing Data using t-SNE. *J. Mach. Learn. Res.* 9,  
1234 2579–2605 (2008).  
1235
- 1236 117. Clark, A. Pillow, Version 9.4.0. Software. <https://pypi.org/project/Pillow/>. (2023).  
1237
- 1238 118. He, K., Zhang, X., Ren, S. & Sun, J. Deep Residual Learning for Image Recognition. *arXiv*  
1239 1512.03385 (2015) doi:10.1109/CVPR.2016.90.  
1240
- 1241 119. Tan, M. & Le, Q. V. EfficientNet: Rethinking Model Scaling for Convolutional Neural  
1242 Networks. *ArXiv abs/1905.11946*, (2019).  
1243
- 1244 120. Cai, L., Zhang, H. & Davis, C. C. PhyloHerb: A high-throughput phylogenomic pipeline  
1245 for processing genome skimming data. *Appl. Plant Sci.* 10, e11475 (2022).  
1246
- 1247 121. Marinho, L. C. et al. Plastomes resolve generic limits within tribe Clusiaceae (Clusiaceae)  
1248 and reveal the new genus *Arawakia*. *Mol. Phylogenet. Evol.* 134, 142–151 (2019).  
1249
- 1250 122. Lyra, G. de M. et al. Phylogenomics, divergence time estimation and trait evolution  
1251 provide a new look into the Gracilariales (Rhodophyta). *Mol. Phylogenet. Evol.* 165, 107294  
1252 (2021).  
1253
- 1254 123. Marinho, L. C. et al. Phylogenetic Relationships of *Tovomita* (Clusiaceae): Carpel  
1255 Number and Geographic Distribution Speak Louder than Venation Pattern. *Syst. Bot.* 46,  
1256 102–108 (2021).  
1257
- 1258 124. Bankevich, A. et al. SPAdes: a new genome assembly algorithm and Its applications to  
1259 single-cell sequencing. *J. Comput. Biol.* 19, 455–477 (2012).

- 1260  
1261 125. Katoh, K. & Standley, D. M. MAFFT multiple sequence alignment software version 7:  
1262 Improvements in performance and usability. *Mol. Biol. Evol.* 30, 772–780 (2013).  
1263  
1264 126. Minh, B. Q. et al. IQ-TREE 2: New Models and Efficient Methods for Phylogenetic  
1265 Inference in the Genomic Era. *Mol. Biol. Evol.* 37, 1530–1534 (2020).  
1266  
1267 127. Jin, J.-J. et al. GetOrganelle: a fast and versatile toolkit for accurate de novo assembly of  
1268 organelle genomes. *Genome Biol.* 21, 241 (2020).  
1269

## 1270 **Data Availability**

1271 New data generated *de novo* genomic for this study is available on NCBI SRA under  
1272 Bioproject PRJNA1052627. All datasets and metadata are thoroughly described in a  
1273 companion Data Descriptor article<sup>100</sup> and deposited at Harvard dataverse  
1274 (<https://doi.org/10.7910/DVN/IMOX0S>), which will be made public upon manuscript  
1275 acceptance. A pretrained model on rfCGRs and varKodes for the all-SRA-taxa dataset is  
1276 available at Huggingface hub  
1277 ([https://huggingface.co/brunoasm/vit\\_large\\_patch32\\_224.NCBI\\_SRA](https://huggingface.co/brunoasm/vit_large_patch32_224.NCBI_SRA))

## 1278 **Code Availability**

1279 Code used in the initial development and test of varKoder is available on Github  
1280 ([https://www.github.com/brunoasm/varkoder\\_development](https://www.github.com/brunoasm/varkoder_development)). All code used to produce  
1281 images is available in the development GitHub repository. The current version of varKoder  
1282 is available at <https://github.com/brunoasm/varKoder>. Both repositories have been  
1283 archived upon manuscript submission at the Figshare repository  
1284 10.6084/m9.figshare.8304017, and will be made public upon acceptance.